The Canadian Mineralogist
Vol. 40, pp. 435-456 (2002)

PLATINUM-GROUP MINERALS AND OTHER DETRITAL COMPONENTS IN THE KAROO-AGE SOMABULA GRAVELS, GWERU, ZIMBABWE

THOMAS OBERTHÜR[§]

Bundesanstalt für Geowissenschaften und Rohstoffe, Stilleweg 2, D–30655 Hannover, Germany

THOROLF W. WEISER[§]

Rischkamp 63, D–30659 Hannover, Germany

LOTHAR GAST

Bundesanstalt für Geowissenschaften und Rohstoffe, Stilleweg 2, D–30655 Hannover, Germany

RONNY SCHOENBERG[¶]

Gruppe Isotopengeologie, Mineralogisch-Petrographisches Institut, Universität Bern,
Erlachstrasse 9a, CH–3012 Bern, Switzerland

DONALD W. DAVIS

Department of Earth Sciences, Royal Ontario Museum, 100 Queen's Park, Toronto, Ontario M5S 2C6, Canada

ABSTRACT

Heavy-mineral concentrates were obtained from a recent exploration campaign for diamond in the Somabula gravels, a paleoplacer of Upper Karoo (Triassic, ~200 Ma) age near Gweru, Zimbabwe. The polymict spectrum of heavy minerals in the Somabula placers comprises staurolite, zircon, monazite, columbite–tantalite, cassiterite, chromite, native gold, platinum-group minerals (PGM), and other components, which suggests derivation from a variety of source lithologies. Age determinations revealed that most of the detrital grains of zircon, monazite and columbite–tantalite originate from Pan-African source rocks. Altogether, 622 detrital PGM grains were identified. Pt and Pt alloys, mainly with Fe, Rh, Pd and Ru, predominate (79%), followed by Os–Ir–Ru–Rh–Pt alloys (10%), rustenburgite [Pt_3Sn] (9%), and rare Pt-rich phases (1%). The compositions of the alloys suggest high-temperature crystallization from a complex Pt–Pd–Rh–Os–Ir–Ru–Fe solid solution in a sulfur-poor magmatic environment, probably mafic–ultramafic rocks. The suite of PGM markedly differs from that of detrital PGM originating from the Great Dyke and from the primary platinum-group element mineralization of the Main Sulfide Zone of the Great Dyke. The mineralogical evidence and Os isotope data obtained for the Os–Ir–Ru alloy rule out the possible derivation of the PGM from the Great Dyke. Instead, they are likely derived from late Archean greenstone belts of the Zimbabwe craton.

Keywords: zircon, monazite, tantalite, U–Pb dating, platinum-group minerals, Pt–Fe alloy, Os–Ir–Ru–Rh–Pt alloys, rustenburgite, gold, Os isotopes, paleoplacer, Karoo Formation, Somabula gravels, Gweru, Zimbabwe.

SOMMAIRE

Nous avons étudié des concentrés de minéraux lourds prélevés lors d'une campagne récente d'exploration pour le diamant ciblée sur les graviers alluvionnaires de Somabula, un paléoplacer d'âge Karoo supérieur (triassique, ~200 Ma) près de Gweru, au Zimbabwe. Le spectre polymicte de minéraux lourds dans les placers de Somabula comprend staurolite, zircon, monazite, columbite–tantalite, cassitérite, chromite, or natif, minéraux du groupe du platine, et autres composants, évidence d'une variété de types de roches à la source. Une étude radiométrique révèle que la plupart des grains détritiques de zircon, monazite, et columbite–tantalite proviennent d'un socle Pan-Africain. En tout, 622 grains de minéraux du groupe du platine ont été identifiés.

[§] *E-mail addresses*: thomas.oberthuer@bgr.de, weiser@wald-info.de
[¶] *Current address*: Department of Earth Sciences, The University of Queensland, Brisbane, 4072, Australia

Le Pt et les alliages de Pt, surtout avec Fe, Rh, Pd et Ru, prédominent (79%); viennent ensuite des alliages de Os–Ir–Ru–Rh–Pt (10%), la rustenburgite [Pt_3Sn] (9%), et des phases platinifères plus rares (1%). La composition des alliages indique une cristallisation à température élevée à partir d'une solution solide complexe Pt–Pd–Rh–Os–Ir–Ru–Fe dans un milieu magmatique à faible teneur en soufre, par exemple des roches mafiques–ultramafiques. La suite de minéraux du groupe du platine diffère de façon marquée des minéraux détritiques dérivés du Great Dyke et des minéraux primaires décrits de la zone principale de sulfures de ce complexe. Les caractéristiques des minéraux et les données isotopiques de l'osmium obtenues pour l'alliage Os–Ir–Ru éliminent toute possibilité que ces minéraux aient été dérivés du massif de Great Dyke. En revanche, ils auraient été dérivés de ceintures de roches vertes de l'Archéen tardif du craton de Zimbabwe.

(Traduit par la Rédaction)

Mots-clés: zircon, monazite, columbite–tantalite, datations U–Pb, minéraux du groupe du platine, alliage Pt–Fe, alliages Os–Ir–Ru–Rh–Pt, rustenburgite, or, isotopes d'osmium, paleoplacer, Formation de Karoo, graviers alluvionnaires de Somabula, Gweru, Zimbabwe.

INTRODUCTION

Diamond was first discovered in the Somabula forest of Zimbabwe in 1903 (Phaup 1958), and no other significant diamondiferous placer deposits are known in Zimbabwe. The diamondiferous gravels were exploited intermittently until about 1930, and since then, production has been sporadic and limited. The diamond output from 1905 to 1956 was recorded as 15,886 carats (Phaup 1958, Gibson 1967). The Somabula gravels are also interesting as they are paleoplacer deposits of Karoo age. Macgregor & Zealley (1921) noted that the heavy minerals of the gravels included "osmiridium and platinum". The availibility of a heavy-mineral concentrate obtained during exploration work of the Trans Hex Group allowed the present investigation of the platinum-group minerals (PGM) in the Somabula paleoplacers. Our aim is (i) to provide a comprehensive characterization of the detrital PGM in the Karoo-age paleoplacers of Somabula, and (ii) to define possible sources of the heavy mineral and PGM assemblage.

GEOLOGICAL SETTING

From about 20 km southwest of Gweru in central Zimbabwe, a tongue of Karoo sediments up to 10 km wide stretches for *ca.* 50 km in a northwesterly direction (Tyndale-Biscoe 1949; Fig. 1). Locally, these sediments reach a thickness of 50 m and show well-developed basal layers of gravel, up to some meters thick. Macgregor & Zealley (1921) noted that the Karoo rocks rest unconformably on an uneven surface of weathered granite. On the basis of fossil plants, Seward & Holttum (1921) assigned the gravels to the Stormberg Series of the Upper Karoo (Triassic, ~200 Ma). The country rocks consist of early to late Archean (*ca.* 3.5–2.6 Ga) granitic and gneissic rocks and greenstone belts (Wilson *et al.* 1995). The Great Dyke, dated at 2575.4 ± 0.7 Ma (Oberthür *et al.* 2002) crops out some 50 km east of the Somabula occurrence (Fig. 1).

The diamondiferous beds are a series of fluviatile and estuarine deposits characterized by beds of gravel with very well rounded pebbles. At the base of the deposit is a "wash" containing a large proportion of rounded crystals of heavy minerals, the most abundant of which is staurolite, which constitutes more than 98% of the heavy minerals (Bührmann 1997). Andalusite, gorceixite, beryl, chromite, chrysoberyl, corundum, garnet, ilmenite, kyanite, rutile, topaz, tourmaline, zircon, native gold and "platinum" also have been reported (Macgregor & Zealley 1921, Macgregor 1941, Harrison 1980). The most characteristic feature of the diamond crystals from Somabula is the faint green tinge of the majority of the stones, which invariably is lost on cutting (Macgregor & Zealley 1921). On average, the stones weigh just under one carat, and the largest diamond of good quality weighs 36¼ carats.

The origin of the placer minerals has been in debate for some time. Macgregor & Zealley (1921) believed that the rivers that deposited the Somabula gravels flowed from the north based on the fact that staurolite, abundant in the Somabula placers, is only found in the Miami mica fields of the Lomagundi district, some 300 km to the north. Harrison (1980) recalled signs of early Karoo glaciation, and speculated that the diamond crystals may have originated from a pipe in the northern part of Zimbabwe, probably in the area of the Zambezi valley, and were transported to the south by a glacier with additions of gravel by fast-flowing rivers from the melted ice. Master (1995) re-evaluated the possible sources of the diamonds and in general supported the hypothesis of Macgregor & Zealley (1921). Master (1995) proposed that the heavy minerals were brought to the Somabula area by a major river system that flowed southward across the Great Dyke and recrossed back in the Somabula region, in the process picking up chromite and platinum-group minerals from the Great Dyke, and gold nuggets from auriferous greenstone deposits. Some chromite may have come from the Archean chromitite deposits of Shurugwi. Master (1995) further proposed

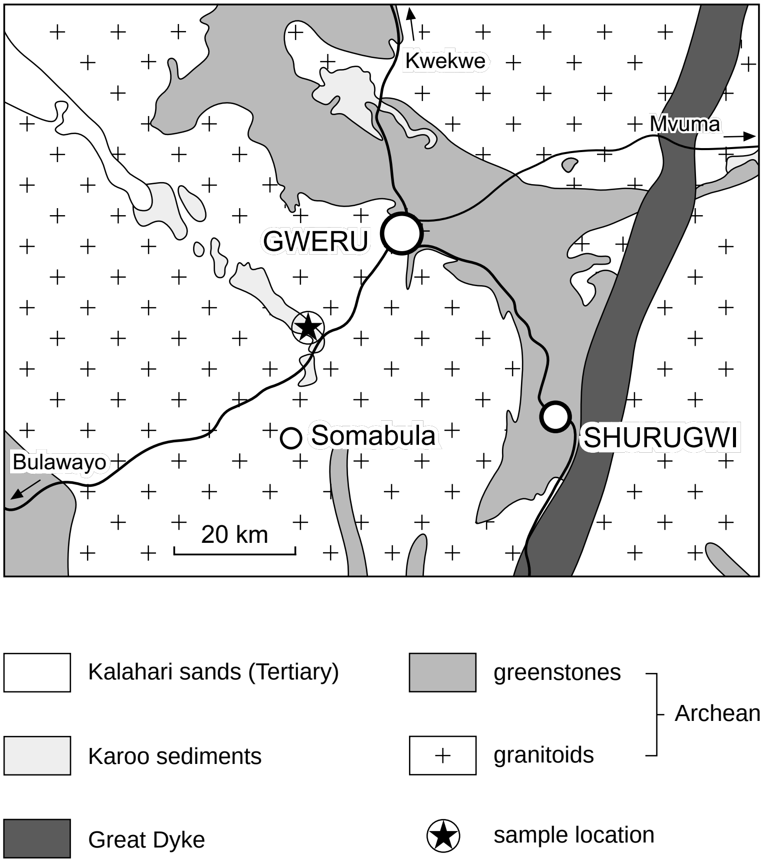

FIG. 1. General geology and regional distribution of Karoo sediments in the Somabula area (redrawn from geological map of Zimbabwe 1:1,000,000, 1996). Sample locality is shown by an asterisks.

that the diamond crystals may originate from undiscovered kimberlites in the Miami district, but he also remarked that the source of the diamond at Somabula remains enigmatic. Sedimentological work of Bührmann (1997) showed that the paleoriver system at Somabula flowed from south to north with an overall gradient of 0.18°, which implies a southerly source of the heavy minerals. This finding contrasts with the views of most earlier authors, who favored sediment sources to the north.

METHODOLOGY

During exploration by the Trans Hex Group between 1994 and 1997, a heavy-mineral concentrate was continuously separated as a by-product of the diamond extraction and stored in barrels at the processing site. We screened 656 kg of this concentrate to <2 mm and treated it in Zimbabwe in 1998. The fine fraction was subsequently washed and panned to obtain fractions of the heaviest minerals. By the above treatment, the densest fraction was reduced to about 10 g of a final concentrate of the heaviest components. The PGM grains, usually having silver metallic colors, and other minerals of interest, were extracted by hand and transferred to SEM sample holders. The grains were inspected with a scanning electron microscope (SEM) equipped with an energy-dispersion system (EDAX). Out of a total of 622 PGM grains detected, 154 grains representing the various groups of PGM were embedded in araldite, polished with diamond powder on a Dürener polisher, and analyzed with a CAMEBAX electron microprobe (EPMA) at BGR. The analytical conditions were: accelerating voltage 20 kV, specimen current 30 nA, and measurement times 10 s. The following standards and X-ray lines were used: Ru$L\alpha$, Rh$L\alpha$, Os$M\alpha$, Ir$L\alpha$, Au$L\alpha$, Ag$L\beta$, Ni$K\alpha$, Se$K\alpha$, Te$L\alpha$, Bi$M\alpha$, Sn$L\alpha$ (metals), Pt$L\alpha$ and Fe$K\alpha$ (synthetic Pt_3Fe alloy), Pd$L\alpha$

(synthetic PdS), S*K*α (synthetic PtS), As*L*α (synthetic GaAs), Pb*M*α (galena), and Sb*L*α (stibnite). Raw data were corrected using the PAP (Pouchou & Pichoir 1991) program supplied by CAMECA. Additional corrections were performed for overlap of the elements Rh, Pd, Ag, Cu, As, and Sb with secondary lines. Detection limits for the elements listed are 0.1 wt.%. Altogether, 232 quantitative electron-microprobe analyses (EPMA) were carried out on the 154 grains of PGM selected and on 15 grains of gold.

Zircon and monazite grains were picked using a binocular microscope. Exterior surfaces of zircon grains were removed by air abrasion. Weights of zircon and monazite fractions, estimated by eye, should be accurate to about ±50%. This affects only U and Pb concentrations, not age information, which depends only on measurements of isotope ratios (Table 1).

Single crystals of zircon and monazite were washed in HNO_3. For all samples, a $^{205}Pb–^{235}U$ spike was added to the dissolution capsules during sample loading. Zircon was dissolved using HF in teflon bombs at 200°C. Monazite dissolution was carried out in a Savillex vial using 6N HCl. For both minerals, purification of Pb and U was carried out in HCl using 0.05 mL anion-exchange columns, following the method of Krogh (1973).

Columbite–tantalite grains were hand-picked using a binocular microscope and mounted on tape into a scanning electron microscope equipped with an energy-dispersion detector. The columbite–tantalite grains showed a predominant Ta peak with subordinate Nb. Six of these grains were selected for analysis, and their weights were estimated using digital imaging software (Matthews & Davis 1999). Sample preparation and dissolution followed the method that Romer & Smeds (1996) used on columbite. The crystals were washed in warm 15% HF for 15 minutes, followed by warm 6N HCl for 1 hour, then warm 7N HNO_3 for 1 hour. No corrosion was visible on any of the crystals as a result of this treatment. Single crystals were dissolved over several days at 110°C in Savillex vials using 30 drops of HF and 1 drop of concentrated H_2SO_4. The solution was dried to remove HF but leaving the H_2SO_4, which is non-volatile. Ten drops of 1N HBr were added, and the covered sample was heated overnight. The solution was poured through a small column packed with 50 μL of anion-exchange resin. Pb is strongly held on the resin under these conditions, whereas U and other elements pass through. The U-bearing solution was re-collected in the Savillex vial. The resin was washed with about 15 drops of 1N HBr. Pb was then eluted into a clean PMP beaker

TABLE 1. U–Pb ISOTOPIC DATA ON ZIRCON, MONAZITE AND TANTALITE FROM THE SOMABULA PALEOPLACER

	Fraction	Weight mg	U ppm	Th/U	Pbcom pg	$^{206}Pb/^{204}Pb$	$^{206}Pb/^{238}U$	$^{207}Pb/^{235}U$	206/238 age Ma	2 σ	207/235 age Ma	2 σ	207/206 age Ma	2 σ	Disc. %
	Zircon and Monazite														
1	1 ab Zrn, lpr, melt incl	0.0100	39	0.31	3.3	1297	0.1721	1.7731	1023.7	4.7	1035.6	5.5	1060.9	12.6	3.8
2	1 Mnz, shiny, rnd, spr	0.0120	1005	13.0	23.8	3302	0.1042	0.8765	638.7	2.1	639.1	2.3	640.3	7.2	0.3
3	1 Mnz, euh, equ	0.0120	826	25.1	24.3	2638	0.1033	0.8652	633.9	2.4	632.9	2.9	629.3	10.0	-0.8
4	1 ab Zrn, euh	0.0050	69	0.57	0.8	2817	0.1020	0.8533	626.2	1.8	626.4	2.4	627.5	8.7	0.2
5	1 Mnz, frosted	0.0160	281	133	15.5	1897	0.1002	0.8329	615.4	2.1	615.2	3.3	614.7	12.7	-0.1
6	1 ab Zrn, resorbed, melt incl	0.0120	64	0.53	4.6	1081	0.0991	0.8271	609.3	1.6	612.0	4.9	621.9	20.6	2.1
7	1 ab Zrn, euh, spr	0.0030	51	0.37	0.2	4364	0.0987	0.8178	606.6	3.2	606.8	2.9	607.4	7.2	0.1
8	1 ab Zrn, frag	0.0160	219	0.29	0.5	39698	0.0902	0.7327	557.0	2.9	558.1	2.4	562.8	2.5	1.1
9	1 ab Zrn, equ, frosted	0.0060	162	0.22	1.6	3540	0.0892	0.7276	550.6	3.1	555.1	2.4	574.0	10.8	4.3
	Columbite–Tantalite														
1	1 tantalite, spr	0.0120	286	0.39	2114.9	62.6	0.57180	14.0894	2915.2	29.5	2755.7	63.4	2640.9	112.9	-12.9
2	1 tantalite, spr	0.0115	80	0.06	28.1	213.6	0.09590	0.7788	590.3	2.6	584.8	21.2	563.4	105.0	-5.0
3	1 tantalite, irreg shape	0.0129	129	-0.02	102.5	100.2	0.08123	0.6420	503.5	4.3	503.6	51.3	504.1	293.9	0.1
4	1 tantalite, spr	0.0114	164	0.00	7.5	1307.8	0.08048	0.6377	499.0	2.0	500.8	4.1	509.4	22.4	2.1
5	1 tantalite, square, flat	0.0112	209	0.02	77.7	166.9	0.07975	0.6358	494.6	2.7	499.7	27.5	522.9	155.3	5.6
6	1 tantalite, equant	0.0227	90	-0.01	33.7	256.4	0.06312	0.4945	394.6	1.7	408.0	14.7	484.5	96.6	19.1

Zrn: zircon grain, Mnz: monazite grain, ab: grain abraded, incl: inclusions, euh: euhedral, rnd: rounded, frag: fragment, spr: short prismatic, lpr: long prismatic, equ: equant. Th/U is calculated from measured $^{206}Pb/^{208}Pb$ and $^{206}Pb/^{238}U$ age. Pbcom is total measured common Pb assuming the isotopic composition of laboratory blank: $^{206}Pb/^{204}Pb$: 18.221, $^{207}Pb/^{204}Pb$: 15.612, $^{208}Pb/^{204}Pb$: 39.360. $^{206}Pb/^{204}Pb$ are measured values corrected for fractionation and spike. $^{206}Pb/^{238}U$ age, $^{207}Pb/^{235}U$ age and $^{207}Pb/^{206}Pb$ age are corrected for ^{230}Th disequilibrium, assuming a magmatic Th/U value of 4.2. %Disc.: percent discordance for the given $^{207}Pb/^{206}Pb$ age. U decay constants are from Jaffey *et al.* (1971).

with 6N HCl. The U solution was heated in the open Savillex vial to drive off the HBr, again leaving the H_2SO_4. This was taken up in 10 drops of 6N HCl and reloaded into the column, which had previously been re-conditioned with 6N HCl. U is strongly absorbed under these conditions. The resin was washed with 30 drops 6N HCl, followed by 10 drops 7N HNO_3. U was eluted back into the Savillex vial using H_2O. A drop of 0.5N H_3PO_4 was added to the Pb and U solutions, which were then dried down.

Pb and U from zircon and monazite were loaded together on Re filaments using silica gel. The Pb and U fractions derived from the tantalite were loaded onto separate filaments. The isotopes were measured using a VG354 mass spectrometer equipped with a Daly ion counter. The samples produced strong, smooth signals for both Pb and U. The data reported are corrected for ion-counter mass discrimination of 0.0007/AMU and a detector dead-time of 23.0 ns. The thermal mass-discrimination correction is 0.0010/AMU. A blank analysis for the tantalite procedure gave a Pb blank of 3.7 pg and a U blank of 1.5 pg. For zircon and monazite, Pb and U blanks were taken to be 1 pg and 0.1 pg, respectively. After subtraction of blank, the results were corrected for common Pb using values from the growth curve of Stacey & Kramers (1975) at the $^{206}Pb/^{238}U$ age of the sample.

Os isotope compositions of PGM grains were analyzed at the University of Bern, Switzerland. Single PGM grains were digested in sealed Carius tubes in reverse aqua regia. After opening the Carius tubes, Os was directly distilled into chilled HBr following the method described by Nägler & Frei (1997). Os isotope compositions were determined on a NuInstruments multicollector inductively coupled plasma – mass spectrometer (MC–ICP–MS) by direct transfer of Os as OsO_4 into the argon stream (Schoenberg *et al.* 2000). The twelve Faraday collector array of the MC–ICP–MS allows simultaneous detection of all Os isotope beams in static measurement mode and also allows the monitoring of other elements that might interfere with Os isotope masses. Monitored isotopes were ^{182}W, ^{185}Re and ^{194}Pt to allow for simulaneous in-run correction of their interfering isotopes ^{186}W, ^{187}Re, ^{190}Pt and ^{192}Pt, respectively. However, purification of Os by distillation (Nägler & Frei 1997) is very efficient, and neither W nor Re nor Pt was detected during the analyses. Os isotope ratios were fractionation-corrected using an exponential law and $^{192}Os/^{188}Os = 3.082614$ (Nier 1937).

MINERALOGY OF THE PLACER

Corroborating and extending earlier findings (Macgregor & Zealley 1921, Phaup 1958, Bührmann 1997), staurolite predominates (>95%) in the heavy-mineral spectrum. Staurolite grains attain several mm across. The grains are dark brown to black and opaque. According to K.-P. Burgath (pers. commun., August 2000), they contain numerous inclusions of quartz, tourmaline, hematite or magnetite, and possibly zircon. The staurolite grains are undeformed, post-kinematic poikiloblastic grains and probably formed under amphibolite-facies conditions of metamorphism (P–T range >515–680°C, >2.5 kbar; Bucher & Frey 1994).

Zircon, monazite, cassiterite, columbite–tantalite, chromite, magnetite, hematite, ilmenite, garnet, corundum, uraninite, thorianite, native gold, and PGM are the main minerals of the heaviest fraction of the concentrate (Fig. 2). Notably, the cassiterite grains come in many different colors (transparent yellowish brown, light yellow, yellow-orange, orange-red to deep red and, rarely opaque and black). Studies by J. Götze (pers. commun., May 1998) showed that the crystals of cassiterite have (i) a low Fe content, (ii) inclusions of Ta-rich columbite, and (iii) relatively monotonous cathodoluminescence spectra, without conspicuous zoning. J. Götze (pers. commun., May 1998) concluded that the cassiterite crystals most probably originate from highly evolved granitic pegmatites.

Grains of gold are far more numerous than PGM grains. The concentrate has an estimated content of about 10 g/t Au, whereas its recalculated Pt content ranges between about 10 and 20 ppb. The grains of gold display a wide range of shapes and sizes (Fig. 2). Flat disks, flakes, rods and also round grains are present, and most grains range in size between 250 μm and 1 mm in longest dimension; the largest grain is 4 mm long. In addition to the discrete grains of gold, thin (<1–5 μm) secondary films and coatings of silver-poor gold were detected on a number of PGM grains. EPMA showed that most of the gold grains are very pure (>99 wt.% Au). However, the concentrate also contains a smaller fraction of gold grains with between 10.6 and 29.6 wt.% Ag. Some of the Ag-rich gold grains have a thin rim depleted in Ag. Other elements sought (Pd, Cu, Fe, Hg and Bi) were below the detection limit, about 0.1 wt.%.

Age dating of zircon, monazite and columbite–tantalite

Three single grains of pale greenish monazite, six single grains of colorless zircon, and six single grains of brownish columbite–tantalite were dated using the U–Pb method. Results of U–Pb isotopic analyses are given in Table 1 (errors at 2σ). Results are plotted on concordia diagrams on Figures 3 and 4. Error ellipses are plotted at 2σ. Average errors in the age are given at 95% confidence levels. Probabilities of fit would be expected to be 50% on average for random data with correctly chosen analytical errors. Errors in the age derived from $^{207}Pb/^{206}Pb$ are quoted at 2σ.

Both zircon and monazite are very fresh. Most grains are rounded or subrounded. A few have frosted surfaces typically produced by detrital transport, but most have smooth reflective surfaces. Regarding zircon and monazite, eight data points are concordant or near-concordant, with a range of $^{206}Pb/^{238}U$ ages between 639 ± 2 Ma and 551 ± 3 Ma (Fig. 3). One zircon crystal gave a distinctly older, slightly discordant data-point with a $^{207}Pb/^{206}Pb$ age of 1061 ± 13 Ma. A line running through this point and the middle of the distribution of the younger crystals of zircon would have an upper concordia intersection of 1100 ± 23 Ma (Fig. 3).

The age range of most of the grains matches that of Pan-African rocks. Since almost all of the zircon and monazite is similar in appearance, these ages may be typical of the whole population. The calculated Th/U values are indicative of a probable magmatic, rather than metamorphic, origin for both zircon and monazite. The high abundance of monazite suggests that the source rocks were derived from crustal melts, such as S-type granitic rocks. The moderate level of discordance of the older zircon, which seems very fresh and is unlikely to have suffered low-temperature loss of Pb, suggests that it has been disturbed by a thermal event. If so, this might indicate that part of the basement to the orogen was about 1100 Ma in age.

Concentrations of uranium in the columbite–tantalite grains are fairly high, but concentrations of common Pb also proved to be generally high and variable. Only one grain yielded a highly radiogenic datum, which is concordant with a $^{206}Pb/^{238}U$ age of 499.0 ± 2.0 Ma (Table 1). The high proportion of common Pb in the other analyses causes a substantial increase in the $^{207}Pb/^{235}U$ errors (Fig. 4). This level of common Pb is well above the blank and may be due to inclusions that are not visible owing to the opaque nature of the grains.

The five youngest data are concordant or nearly so, but have $^{206}Pb/^{238}U$ ages that vary in the range 395–590 Ma (Table 1, Fig. 4). Three cluster around 500 Ma but are slightly outside of error range. A sixth grain yielded a much older datum, with a $^{206}Pb/^{238}U$ age of 2915 ± 30 Ma. However, this is distinctly to the left of concordia, suggesting either isotopic disturbance or an incorrect choice of correction for common Pb. This sample also showed an extremely high level of common Pb compared to the others. If the discordance is due to isotopic disturbance (differential mobility of U and Pb), then the true age of the grain may be closer to the $^{207}Pb/^{206}Pb$ age of 2641 ± 113 Ma. The discordance would be much reduced if the analysis were corrected for a more recent common Pb isotopic composition, and the age would approach 2600 Ma. This approach would also reduce the calculated Th/U value to nearly zero, in accord with the other analyses.

Romer & Smeds (1996) observed that HF treatment did not differentially leach Pb or U from columbite. However, the roughly linear trend of the younger data from Somabula and the reversely discordant older datum suggest that U and Pb may have been mobile. If the spread of ages for the younger data is due to recent U–Pb disturbance, the upper concordia intersection of a zero-age line through them should give the best estimate of age. This is 511 ± 20 Ma (Fig. 4). The line is not well

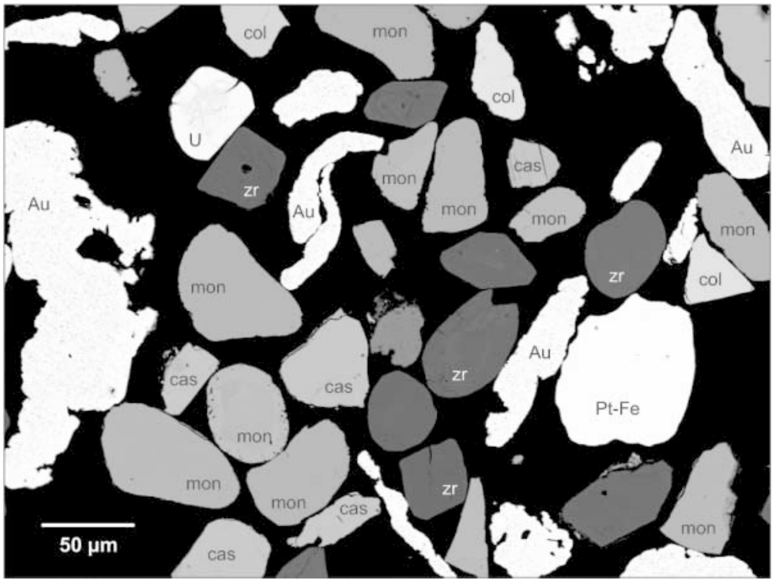

FIG. 2. Back-scattered electon image of part of the final heavy-mineral concentrate from Somabula. Polished section of sieve fraction <125 µm. White grains are gold (Au) except one grain each of Pt–Fe alloy (Pt–Fe) and uraninite (U). Other components are zircon (zr, darkest grey), monazite (mon), cassiterite (cas), and columbite–tantalite (col).

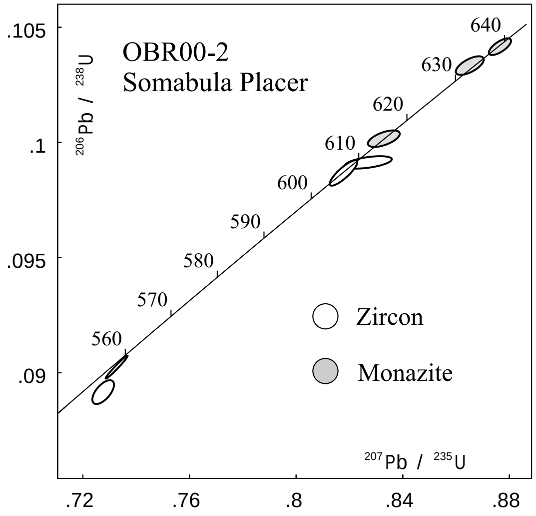

FIG. 3. U–Pb concordia diagram showing data for zircon and monazite. Data are numbered according to entries in Table 1.

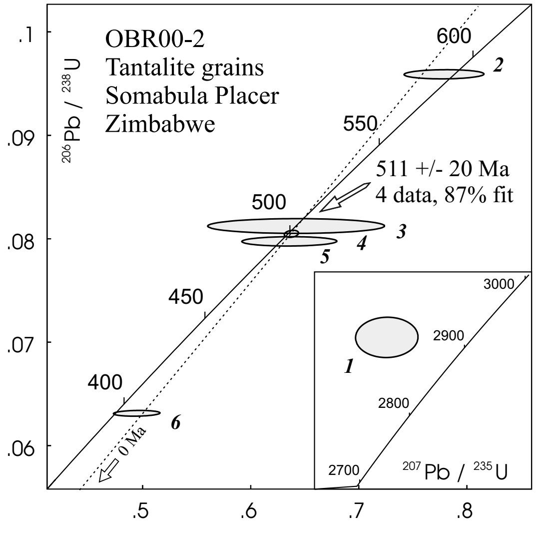

FIG. 4. U–Pb concordia diagram showing data for columbite–tantalite. Data are numbered according to entries in Table 1.

constrained because most of the data have large ^{207}Pb/^{235}U errors. This is the most conservative interpretation, but it is also possible that each grain has a different age, as with the zircon and monazite grains from this sample. Columbite–tantalite grain 1 (Table 1), despite its relatively high uncertainty, clearly has a much older late Archean age.

Collectively, the age range of most of the zircon, monazite and columbite–tantalite grains matches that of Pan-African rocks. Therefore, the Pan-African Zambezi and Mozambique belts to the north and east have to be envisaged as potential sources.

Platinum-group minerals (*PGM*)

A total of 622 PGM grains were extracted from the heavy-mineral concentrates. Their morphology and composition were studied under the SEM with an attached energy-dispersion analytical system (EDAX). In all, 154 selected PGM grains were analyzed by EPMA. The grain sizes (maximum diameters) range from *ca.* 100 to 850 μm. The spectrum of PGM consists of Pt and Pt alloys with Fe, Rh, Pd, and Ru (79%), Os–Ir–Ru–Rh–Pt alloys (10%), rustenburgite [Pt_3Sn] (9%) and other Pt–rich compounds (1%). Most PGM grains are monomineralic. Intergrowths of different PGM are rare, and even rarer are mineral inclusions in the PGM.

Pt and Pt alloys

The following mineral proportions by numbers were obtained by SEM surface analysis using the energy-dispersion system (EDAX) attached to the SEM (altogether, 492 Pt-rich grains): 43.3% Pt, 49.2% Pt–Fe alloy, 4.1% Pt–Rh–Fe alloy, 2.2% Pt–Pd–Fe alloy, and 1.2% Pt–Ru–Fe alloy. Our selection from these 492 grains for EPMA was somewhat biased toward grains having unusual compositions.

The grains of *Pt and Pt–Pd alloy* are very similar in external appearance. They are the ”softest” PGM grains and are mostly present as flat disks, some with contorted edges. Flakes, irregular particles and rarer rounded grains may have slightly porous parts and smaller cavities. Typically, the surfaces of the Pt and Pt–Pd alloy grains are mostly rough. In polished sections, many grains display variable internal porosity. The grains of Pt and Pt–Pd alloy reach the largest sizes (up to 850 μm) of all PGM grains (Figs. 5a, 6a). Occasionally, a thin crust of iron hydroxide covers parts of the grains. Other grains locally have a thin (up to 5 μm) film of Ag-poor gold deposited on their surface or intergrown with gold (Fig. 6c).

Grains of Pt–Fe alloy attain 600 μm across and are mainly equidimensional, and commonly well-rounded (“potato shapes”), with smooth convex, polished, silver-white surfaces. Some grains have orthogonal outlines (“bricks”) with polished surfaces and rounded corners (Fig. 5b), and other grains show thin cracks. Internally, the Pt–Fe grains are generally homogeneous. Intergrowths with Pt–Rh–Fe alloy (Fig. 6d) or with rustenburgite (Fig. 6e) are rare.

The rarer alloys containing *Pt–Pd–Fe*, *Pt–Rh–Fe*, and *Pt–Ru–Fe* are mainly represented by round grains, either with smooth surfaces or with etch pits on their surfaces. In general, they have a similar appearance to

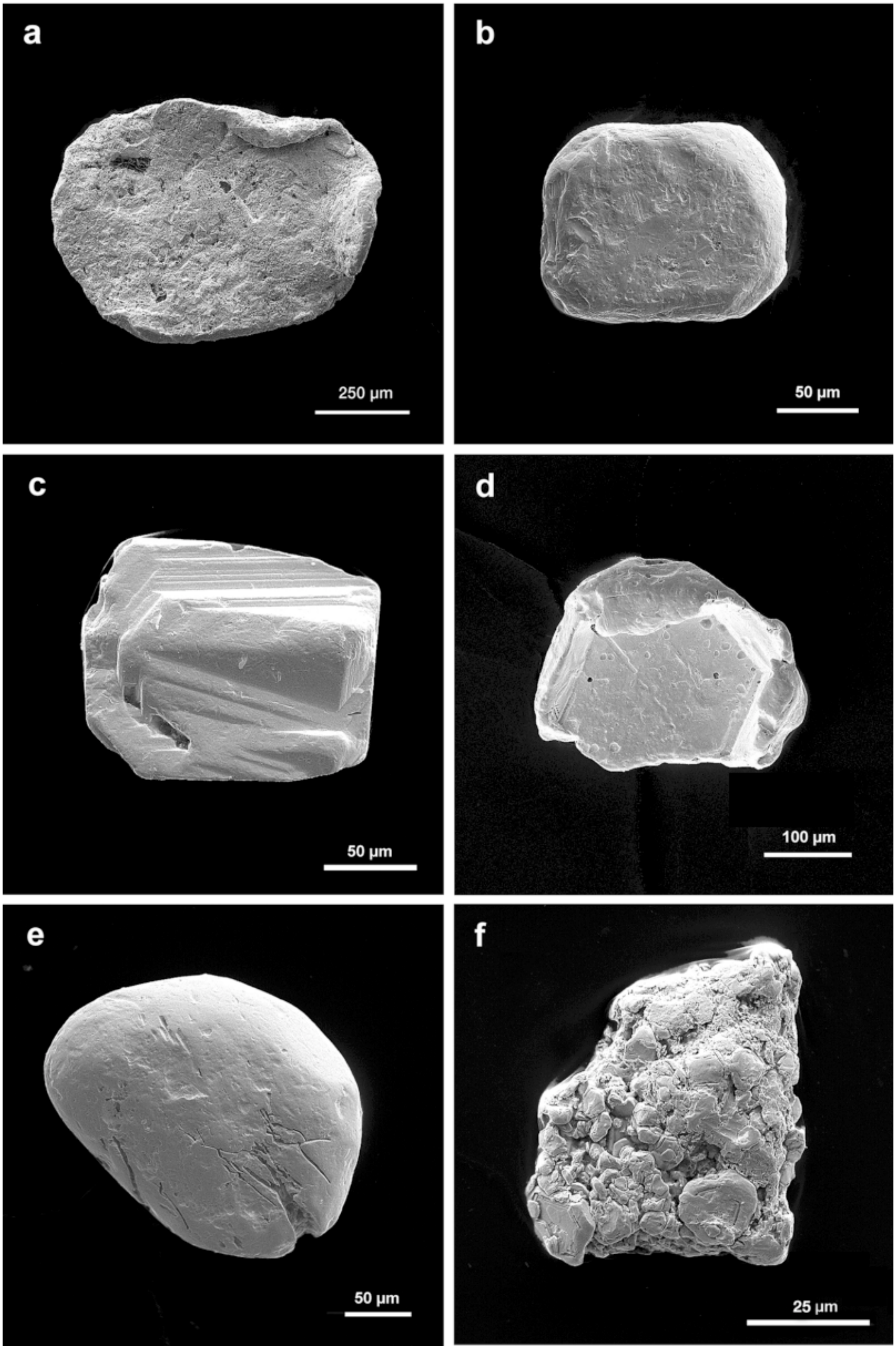
a
250 µm
b
50 µm
c
50 µm
d
100 µm
e
50 µm
f
25 µm

TABLE 2. SELECTED ELECTRON-MICROPROBE DATA PERTAINING TO Pt AND Pt–Pd–Ru–Rh–Fe ALLOYS, SOMABULA GRAVELS, ZIMBABWE

Anal.	67	1	2	21	31	185	27	84	158	206	212	215	173	181	190	195	165	172
Pt	100.07	88.72	78.61	89.51	85.12	86.73	82.68	68.38	58.36	53.71	66.29	57.05	43.58	72.12	65.00	85.40	57.80	52.90
Pd	n.d.	9.53	20.11	n.d.	0.91	0.21	4.84	13.57	22.27	3.19	2.89	n.d.	0.78	n.d.	n.d.	0.88	0.88	0.64
Ru	n.d.	n.d.	n.d.	n.d.	n.d.	n.d.	n.d.	2.87	0.61	19.95	5.19	23.71	0.19	3.78	2.49	n.d.	0.78	n.d.
Rh	n.d.	n.d.	n.d.	n.d.	n.d.	0.64	0.28	1.86	3.10	3.94	3.86	3.58	26.06	17.46	13.72	3.20	14.07	17.75
Os	n.d.	n.d.	n.d.	n.d.	n.d.	n.d.	n.d.	n.d.	n.d.	2.61	1.13	1.73	n.d.	0.66	3.74	n.d.	n.d.	n.d.
Ir	n.d.	n.d.	n.d.	n.d.	0.24	3.13	1.21	1.20	0.31	9.50	11.80	8.38	1.57	1.16	6.00	n.d.	0.17	1.12
Fe	n.d.	n.d.	n.d.	8.60	11.08	8.27	9.76	6.76	10.27	5.52	7.10	3.65	20.07	3.73	7.32	9.55	18.99	18.56
Cu	n.d.	n.d.	n.d.	n.d.	1.17	0.41	0.52	3.96	2.10	0.39	0.35	0.31	0.37	n.d.	n.d.	0.30	0.39	0.75
Ni	n.d.	n.d.	n.d.	n.d.	0.66	n.d.	0.44	0.45	0.57	0.30	0.48	0.36	5.96	n.d.	0.42	n.d.	5.50	6.45
Au	n.d.	1.09	1.17	n.d.	n.d.	n.d.	n.d.	n.d.	n.d.	n.d.	n.d.	n.d.	n.d.	n.d.	n.d.	n.d.	n.d.	n.d.
Sn	n.d.	n.d.	n.d.	1.18	n.d.	n.d.	n.d.	n.d.	n.d.	n.d.	n.d.	n.d.	n.d.	n.d.	n.d.	n.d.	n.d.	n.d.
Total	100.07	99.34	99.89	99.29	99.18	99.39	99.73	99.05	97.59	99.11	99.09	98.77	98.58	98.91	98.69	99.33	98.58	98.17
Pt	1.000	0.827	0.674	0.737	0.647	0.713	0.634	0.486	0.387	0.385	0.512	0.423	0.233	0.566	0.490	0.670	0.333	0.297
Pd	-	0.163	0.316	-	0.013	0.003	0.068	0.177	0.271	0.042	0.041	-	0.008	-	-	0.013	0.009	0.007
Ru	-	-	-	-	-	-	-	0.039	0.008	0.276	0.077	0.340	0.002	0.057	0.036	-	0.009	-
Rh	-	-	-	-	-	0.010	0.004	0.025	0.039	0.054	0.057	0.050	0.264	0.260	0.196	0.048	0.154	0.190
Os	-	-	-	-	-	-	-	-	-	0.019	0.009	0.013	-	0.005	0.029	-	-	-
Ir	-	-	-	-	0.002	0.026	0.009	0.009	0.002	0.069	0.093	0.063	0.009	0.009	0.046	-	0.001	0.006
Fe	-	-	-	0.247	0.294	0.238	0.261	0.168	0.238	0.138	0.192	0.095	0.374	0.102	0.193	0.262	0.382	0.366
Cu	-	-	-	-	0.027	0.010	0.012	0.086	0.043	0.009	0.008	0.007	0.006	-	-	0.007	0.007	0.013
Ni	-	-	-	-	0.017	-	0.011	0.011	0.013	0.007	0.012	0.009	0.106	-	0.011	-	0.105	0.121
Au	-	0.010	0.010	-	-	-	-	-	-	-	-	-	-	-	-	-	-	-
Sn	-	-	-	0.016	-	-	-	-	-	-	-	-	-	-	-	-	-	-

Compositions are first expressed in wt.%, then in atoms per formula unit (*apfu*); n.d.: not detected. Column headings: 67: platinum, 1, 2: Pt–Pd alloy, 21, 31, 185: Pt–Fe alloy, 27, 84, 158: Pt–Pd–Fe alloy, 206, 212, 215: Pt–Ru–Fe alloy, 173, 181, 190, 195: Pt–Rh–Fe alloy, 165, 172: Pt–Fe alloy.

the grains of Pt–Fe alloy. They reach about 350 μm in size. These alloys host the few exsolution lamellae and inclusions observed. Figure 7b shows lamellae of osmium in Pt–Pd–Fe alloy, and Figure 7c, oriented exsolution-induced lamellae of ruthenium in Pt–Rh–Fe alloy.

Figures 8a and 8b show the results of 99 analyses of grains of Pt and Pt alloy, in at.%, in terms of Pt – (Pd + Ru + Rh + Os + Ir) – (Fe + Cu + Ni). Figure 8a contains the compositions of (i) Pt, (ii) Pt–Pd alloy, (iii) Pt–Pd–Fe alloy (defined as: concentration of Pd > Ru, Rh, Os or Ir) , and (iv) Pt–Fe alloy (Ru, Os or Ir <3 at.%). Figure 8b shows the compositions of (i) Pt–Rh–Fe alloy (concentration of Rh > Pd, Ru, Os or Ir; triangles), (ii) Pt–Ru–Fe alloy (concentration of Ru > Pd, Rh, Os or Ir; squares), and (iii) one grain with Ir > Pd, Rh, Ru or Os (diamond).

FIG. 5. Scanning electron microscope (SEM) images of PGM grains from Somabula. a. Large discoid, flat and slightly porous grain of Pt–Pd alloy with contorted rims. b. Hypidiomorphic grain of Pt–Fe alloy. c. Grain of rustenburgite showing growth steps and only little abrasion. d. Rounded grain of iridium with bent edges and internal negative hexagonal crystal (probably formerly a platelet of osmium). e. Well-rounded grain of osmium. f. Aggregate consisting of hexagonal platelets of osmium cemented by a matrix of Pt–Fe alloy.

Chemically, the *Pt* grains are very pure (>98 wt.% Pt; Table 2, no. 67; Fig. 8a) and only rarely contain traces of Ir (up to 0.7 wt.%; Table 2, no. 51), Fe (up to 0.5 wt.%), or Rh (up to 0.2 wt.%). The grains of *Pt–Pd alloy* show a wide range of Pd contents (up to 20.1 wt.%). Some grains are characterized by alternating Pd-poor and Pd-rich zones and carry up to 1.2 wt.% Au (Fig. 7a, Table 2, nos. 1 and 2).

The *Pt–Fe alloy* grains may contain up to 0.9 wt.% Pd, 0.4 wt.% Rh, and 1.3 wt.% Sn (Table 2, no. 26). Contents of Fe + Cu + Ni range between 25 and 29 at.%. Therefore, the compositions plot in the range between Pt_3Fe and Pt_2Fe (Fig. 8a). Cabri *et al.* (1996) observed a

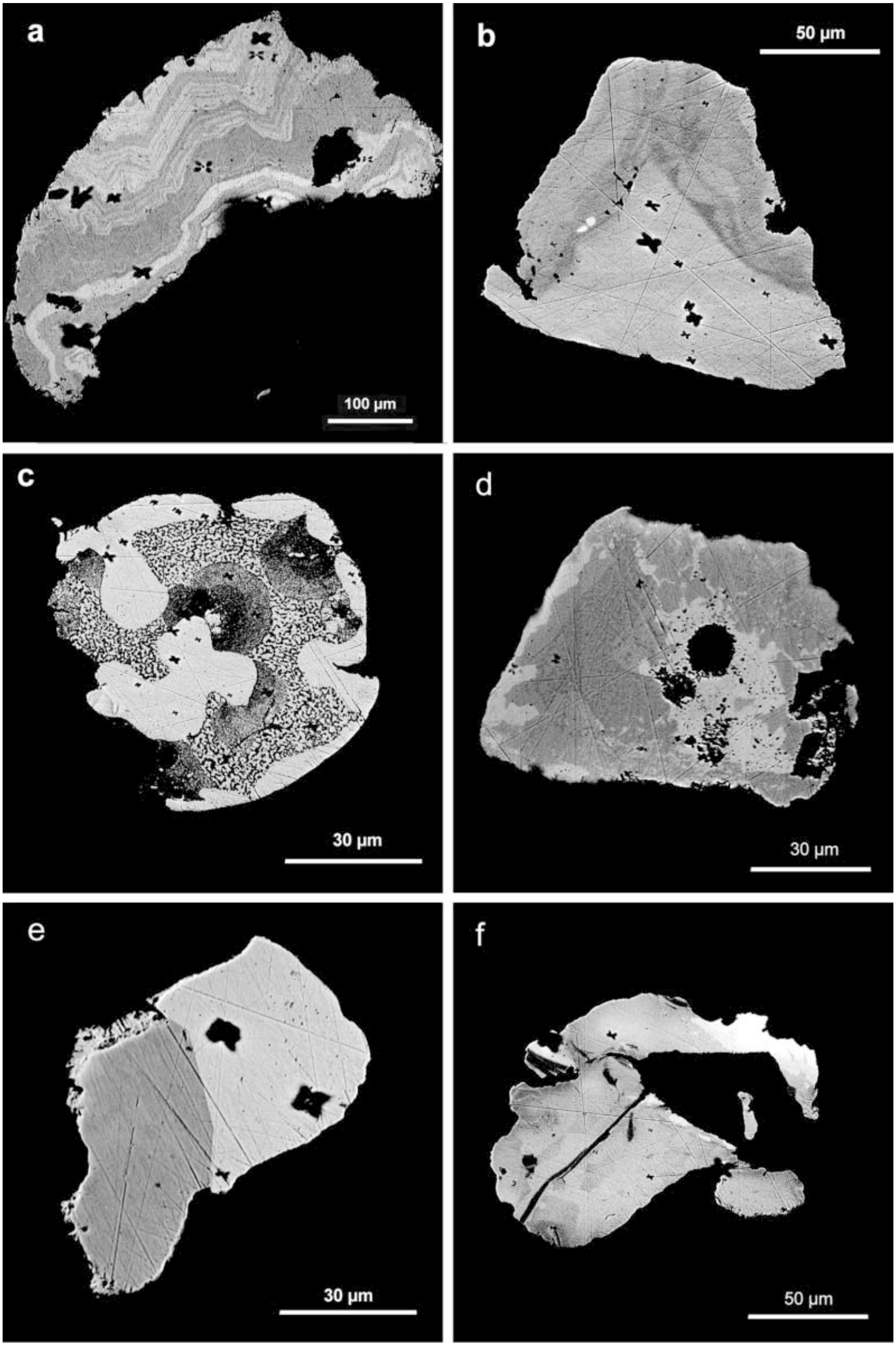
a
100 µm
b
50 µm
c
30 µm
d
30 µm
e
30 µm
f
50 µm

similar narrow compositional range of Pt–Fe alloy only in samples from the Rio Condoto area, Colombia.

The grains of *Pt–Pd–Fe alloy* (Fig. 8a) mainly plot into a field bordered by Pt_3Fe and Pt_2Fe. Up to 22.3 wt.% Pd substitutes for Pt (Table 2, no. 158). Minor elements amount to 3.2 wt.% Ir, 2.4 wt.% Ru, 1.5 wt.% Rh, and 0.2 wt.% Os.

Rhodium substitutes for Pt in the *Pt–Rh–Fe alloy* (Fig. 8b), although to a lesser degree than Pd in the grains of Pt–Pd–Fe alloy. Figure 6d shows an intergrowth of Pt–Fe alloy in the core and Pt–Rh–Fe alloy with varying composition in the rim. The high content of 6.0 wt.% Ir, 3.7 wt.% Os, and 2.5 wt.% Ru in this alloy (Table 2, no. 190) may be due to submicroscopic inclusions of Os–Ir–Ru alloy, although the surface has a homogeneous appearance both under reflected light and in the BSE image. The only sulfides and tellurides of unnamed phases (see below, Table 6, nos. 223 and 224) observed are inclusions in Pt–Rh–Fe alloy (Fig. 7d). Notably, the compositions of some grains plot distinctly outside the field bordered by Pt_3Fe and Pt_2Fe (Fig. 8b).

A second group of *Pt–Rh–Fe alloy* plots close to the line of PtFe (tetraferroplatinum) compositions (Fig. 8b, Table 2, nos. 165, 172, 173). In these grains, Rh substitutes for Pt (maximum 26.1 wt.% Rh), and at the same time, Fe is replaced by substantial amounts of Ni (up to 6.4 wt.% Ni). One grain (Table 2, no. 173) contains more Rh than Pt, resulting in the formula $(Rh_{0.54}Pt_{0.47}Pd_{0.02}Ir_{0.02})_{\Sigma 1.05}(Fe_{0.75}Cu_{0.01}Ni_{0.21})_{\Sigma 0.97}$. The phase could be the Rh equivalent of tetraferroplatinum or of ferronickelplatinum.

Grains of ruthenium-rich *Pt–Ru–Fe alloy* contain up to 23.7 wt.% Ru. They are shown as squares in Figure 8b, and typical results of analyses are given in Table 2, no. 206 and 215. The composition of one Ir-rich grain (11.8 wt.% Ir) is shown in Figure 8b (diamond) and given in Table 2 (no. 212).

Similarly unusual Pt alloys, in this case with elevated contents of Ru (up to 21.9 wt.%), Ir (up to 26.8 wt.%) and Os (up to 12.9 wt.%), were reported by Tolstykh *et al.* (1999) from northwestern Salair, Russia. In general, however, similar exotic compositions of Pt–Fe alloys with highly elevated contents of Pd, Ru and, above all, Rh, have only sporadically been reported previously (*cf.* Cabri *et al.* 1996), making these grains somewhat enigmatic constituents of the Somabula placers.

Fig. 6. Back-scattered electron images of PGM and gold alloys from Somabula. a. Rhythmically zoned grain of $Pt_{83}Pd_{17}$ alloy (light grey) and $Pt_{68}Pd_{32}$ alloy (darker grey). b. Schlieren-like grain of Pt (light grey), $Pt_{69}Fe_{31}$ alloy (medium grey), and $Pt_{66}Fe_{34}$ alloy (dark grey) with two roundish inclusions of Au–Pd–Cu alloy (white). c. Composite grain of Pt (homogeneous areas) and corroded $Pt_{84}Au_{16}$ alloy. d. Intergrowth of $Pt_{75}Fe_{25}$ alloy (light grey), $Pt_{57}Rh_{18}Fe_{25}$ alloy (medium grey), and $Pt_{49}Rh_{31}Fe_{20}$ alloy (dark grey). e. Composite grain of Pt–Fe alloy (light grey) and Pd-bearing rustenburgite (dark grey). f. Intergrowth of Ru-rich Pt–Fe alloy (darker grey), Pd-rich Pt–Fe alloy (light grey), and iridium (white).

Hongshiite

Five grains of hongshiite were detected; they are elongate and roundish, with a diameter between *ca.* 150 and 270 μm. One grain has a smooth surface, the others show signs of etching. Chemical compositions are close to PtCu for most grains; however, one grain has an elevated content of Rh (3.8 wt.%), Pd (2.0 wt.%), and Ir (1.2 wt.%) (Table 3, no. 214).

Pt–Pd–Au–Cu alloy

Grains of alloy in the system Pt–Pd–Au–(Cu) are very rare in the samples from Somabula. One rounded single grain 200 μm long consists of 48.7 wt.% Pt, 9.9 wt.% Pd, and 40.8 wt.% Au. The formula corresponds to $(Pt_{0.45}Pd_{0.17})_{\Sigma 0.62}Au_{0.38}$ (Table 4, no. 6).

Figure 6c shows a composite grain of Pt alloy and corroded Pt–Au alloy 150 μm in diameter. Electron-microprobe analyses of the latter gave a composition of 82.7 wt.% Pt and 15.9 wt.% Au. No other elements were detected (Table 4, no. 47). This composition corresponds to the formula $Pt_{0.84}Au_{0.16}$. According to Hansen & Anderko (1958), such solid solution is stable only above 1050°C.

TABLE 3. SELECTED ELECTRON-MICROPROBE DATA PERTAINING TO HONGSHIITE AND RUSTENBURGITE, SOMABULA GRAVELS, ZIMBABWE

Anal. no.	18	150	214	10	65	101	139	161
Ru wt.%	n.d.	n.d.	n.d.	n.d.	n.d.	n.d.	n.d.	n.d.
Rh	n.d.	n.d.	3.81	n.d.	n.d.	n.d.	n.d.	n.d.
Pd	0.52	0.97	2.04	n.d.	5.10	n.d.	17.04	12.77
Os	n.d.	n.d.	n.d.	n.d.	n.d.	n.d.	n.d.	n.d.
Ir	n.d.	n.d.	1.16	n.d.	n.d.	n.d.	n.d.	n.d.
Pt	73.97	72.89	66.86	83.21	76.81	82.00	63.74	67.40
Fe	n.d.	n.d.	n.d.	0.27	n.d.	n.d.	n.d.	n.d.
Cu	24.20	24.63	24.40	n.d.	n.d.	n.d.	n.d.	n.d.
Ni	n.d.	n.d.	n.d.	n.d.	n.d.	n.d.	n.d.	n.d.
Sn	n.d.	n.d.	n.d.	16.66	17.43	17.16	19.39	19.35
Total	98.69	98.49	98.27	100.14	99.34	99.16	100.17	99.52
Ru *apfu*	-	-	-	-	-	-	-	-
Rh	-	-	0.094	-	-	-	-	-
Pd	0.013	0.024	0.049	-	0.326	-	0.985	0.764
Os	-	-	-	-	-	-	-	-
Ir	-	-	0.015	-	-	-	-	-
Pt	0.992	0.970	0.869	2.984	2.676	2.976	2.010	2.199
Fe	-	-	-	0.034	-	-	-	-
Cu	0.995	1.006	0.973	-	-	-	-	-
Ni	-	-	-	-	-	-	-	-
Sn	-	-	-	0.982	0.998	1.024	1.005	1.037

n.d.: not detected, *apfu*: atoms per formula unit.

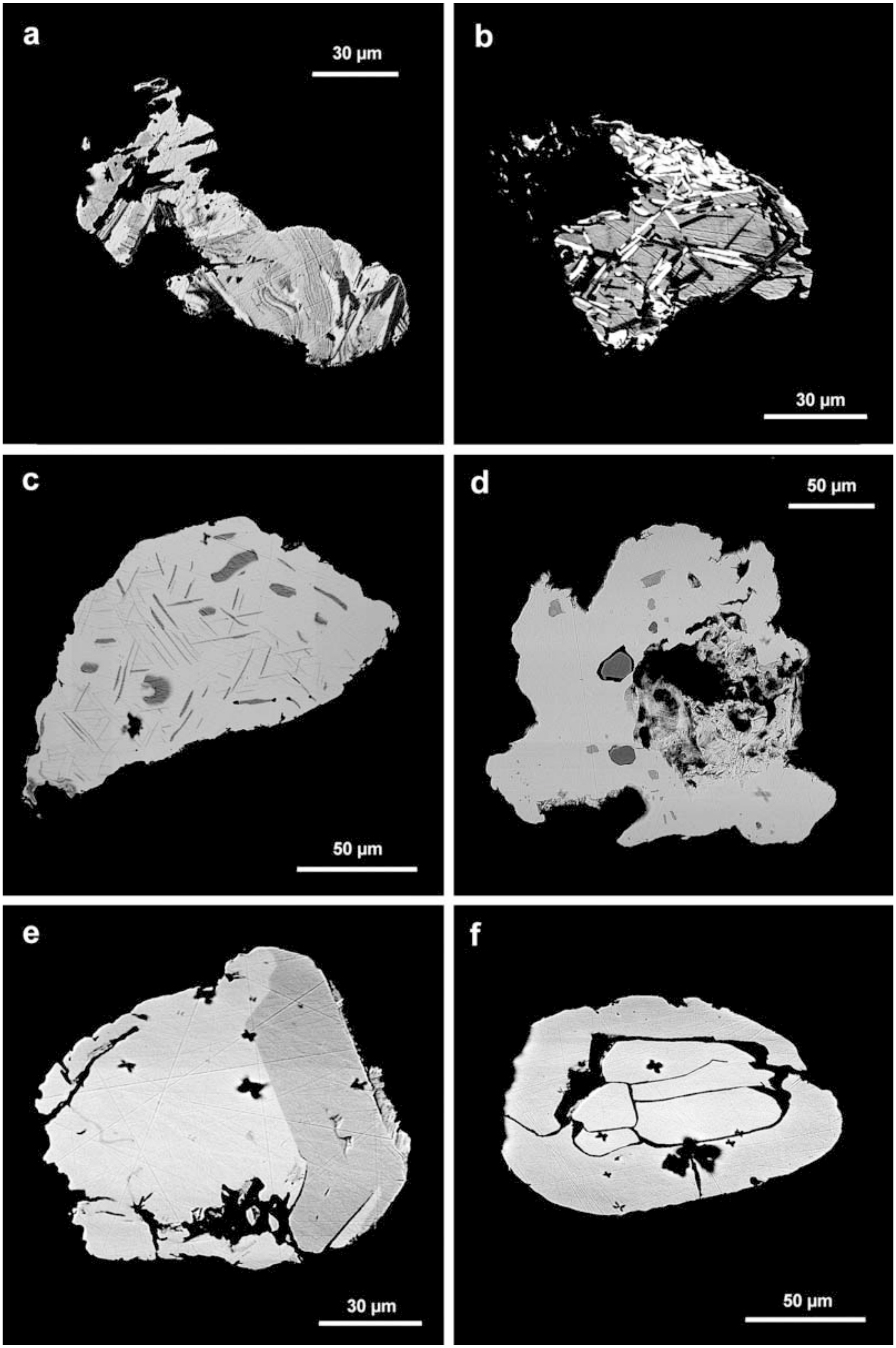
a
30 µm
b
30 µm
c
50 µm
d
50 µm
e
30 µm
f
50 µm

Droplike inclusions in Pt–Fe alloy (Fig. 6b) have a composition of an alloy in the system Pd–Pt–Au–Cu. They contain 7.6 wt.% Pd, 2.9 wt.% Pt, 5.0 wt.% Cu, 0.2 wt.% Fe, 83.3 wt.% Au, and 0.3 wt.% Ag. The formula is calculated to be $(Pd_{0.48}Pt_{0.10}Cu_{0.53}Fe_{0.03})_{\Sigma1.14}$ $(Au_{2.84}Ag_{0.01})_{\Sigma2.85}$, or, ideally Au_3Pd (Table 4, no. 33).

Rustenburgite

This is the first report of rustenburgite as a ubiquitous detrital component in placers at Somabula. Detrital rustenburgite in placers was previously only reported by Törnroos *et al.* (1998) from Finnish Lapland.

The individual grains mostly have a smooth surface and are variably rounded. Some grains show cavities or negative cubic crystals on their surfaces. Some well-crystallized grains, even cubes, also are present (Fig. 5c). The grains mainly have sizes around 100 μm (maximum *ca.* 250 μm), and some grains of rustenburgite were found to be intergrown with Pt–Fe alloy (Fig. 7e).

Most grains are close to the ideal composition (Pt_3Sn). Some grains, however, also show considerable contents of the atokite component Pd_3Sn, indicating substantial solid-solution between rustenburgite and atokite (Fig. 6e, Table 3, nos. 65, 139 and 161).

Grains of Os–Ir–Ru–Rh–Pt alloy

Many grains of Os–Ir–Ru–Pt–Rh alloy are characterized by excellent rounding ("potato"- and "bean"-shaped, rarer flat disks), smooth surfaces, and sizes of up to 350 μm (Fig. 5e). Os-rich grains occasionally display a hexagonal outline (Fig. 5d). Under the SEM, we found a number of coarse intergrowths of Os plates with Pt–Fe alloy (Fig. 5f), and of Ru plates (70 and 150 μm) with Pt–Fe–Rh alloy. In reflected light, the grains of Os–Ir–Ru–Pt–Rh alloy are mostly cream-white with a light bluish tinge and variably anisotropic depending on crystal orientation. Cubic crystals are subordinate. Most grains are optically homogeneous, both under reflected light and in back-scattered electron images. They are devoid of inclusions, and composite grains of various alloys are rare. Exsolution lamellae of osmium and ruthenium were detected in only three grains of Pt–Pd–Fe and Pt–Rh–Fe alloy (Figs. 7b, c).

EPMA of the individual grains show the presence of phases in the systems Os–Ir–Ru (Fig. 9a), Rh–Ru–Pt (Fig. 9b), Rh–Ru–Ir (Fig. 9b), Ru–Ir–Pt (Fig. 9c), Ir–Os–Pt, Ru–Os–Pt, and Os–Ir–Rh. Osmium is the dominant phase (44%), followed by ruthenium (25%) and iridium (23%). Rutheniridosmine and platinum alloy, representing 4% each, are subordinate. Only single data-points plot into the other triangular diagrams mentioned above. In 27% of the analyzed grains, Rh is the third element and substitutes significantly for Os, Ir or Ru in the various phases.

The composition of osmium varies between 40.6 and 68.8 at.% Os, 11.1 and 46.1 at.% Ir, and 3.3 and 38.9 at.% Ru (Fig. 9a). The grains furthermore contain up to 1.9 wt.% Rh, 1.8 wt.% Pt, 0.26 wt.% Pd, and only occasionally up to 1.3 wt.% Fe. Lamellae of osmium in Pt–Pd–Fe alloy have the composition $Os_{0.65}Ir_{0.19}Ru_{0.16}$ and contain traces of Pt (4.2 wt.%) and Fe (0.2 wt.%), with no significant difference in composition compared to the single grains of osmium.

The grains of ruthenium are mostly Rh-rich and plot in the Rh–Ru–Pt diagram (Fig. 9b). To our knowledge (*cf.* Cabri *et al.* 1996), these are the first minerals to be reported in this system. Only a few grains have compositions plotting in the field of Os–Ir–Ru (Fig. 9a) and Os–Ru–Pt alloys. Lamellae in grains of Pt–Pd–Fe and Pt–Rh–Fe alloy represent an alloy in the system Ru–Ir–Pt (Fig. 7c, Table 5, nos. 198 and 209). Figure 7e shows a composite grain of coexisting Rh–Ru–Pt and Os–Ru–Pt alloys (Table 5, nos. 74 and 75). The composition of the grains of ruthenium in the Rh–Ru–Pt field varies normally between 50.6 and 87.6 at.% Ru, 5.7 and 36.8 at.% Pt, and 6.7 to 12.6 at.% Rh (Fig. 9b). Maximum contents of other elements reach up to 10.5 wt.% Os, 9.9 wt.% Ir, 0.4 wt.% Pd, and 0.4 wt.% Fe. Some grains

Fig. 7. Back-scattered electron images of PGM alloys from Somabula. a. Intergrowth of homogeneous Pt–Pd–Fe alloy (white) and schlieren-like Pt–Ru–Fe alloy (middle and dark grey) and lamellae of ruthenium (darkest grey). b. Pt–Pd–Rh–Ru–Fe alloy (medium grey) with lamellae of osmium (white). c. Pt–Rh–Fe alloy (medium grey) with oriented inclusions and exsolution lamellae of ruthenium (dark grey). d. Pt–Rh–Fe alloy with inclusions of unnamed Rh_3Te_2 (light grey, soft) and unnamed RhS (dark grey, hard). e. Composite grain of Ru–Rh–Pt alloy (light) and Ru–Os–Pt alloy (dark). f. Composite grain of osmium (core) enclosed by iridium (rim).

TABLE 4. SELECTED ELECTRON-MICROPROBE DATA PERTAINING TO PGE–Au ALLOYS, SOMABULA GRAVELS, ZIMBABWE

Anal. No.	6	47	33		6	47	33
Ru wt.%	n.d.	n.d.	n.d.	Ru *apfu*	-	-	-
Rh	n.d.	n.d.	n.d.	Rh	-	-	-
Pd	9.89	n.d.	7.59	Pd	0.168	-	0.479
Os	n.d.	n.d.	n.d.	Os	-	-	-
Ir	n.d.	n.d.	n.d.	Ir	-	-	-
Pt	48.70	82.66	2.89	Pt	0.453	0.836	0.100
Fe	n.d.	n.d.	0.25	Fe	-	-	0.030
Cu	n.d.	n.d.	5.04	Cu	-	-	0.533
Ni	n.d.	n.d.	n.d.	Ni	-	-	-
Au	40.78	15.94	83.32	Au	0.376	0.160	2.842
Ag	n.d.	n.d.	0.27	Ag	-	-	0.017
Total	99.37	98.60	99.36				

n.d.: not detected, *apfu*: atoms per formula unit.

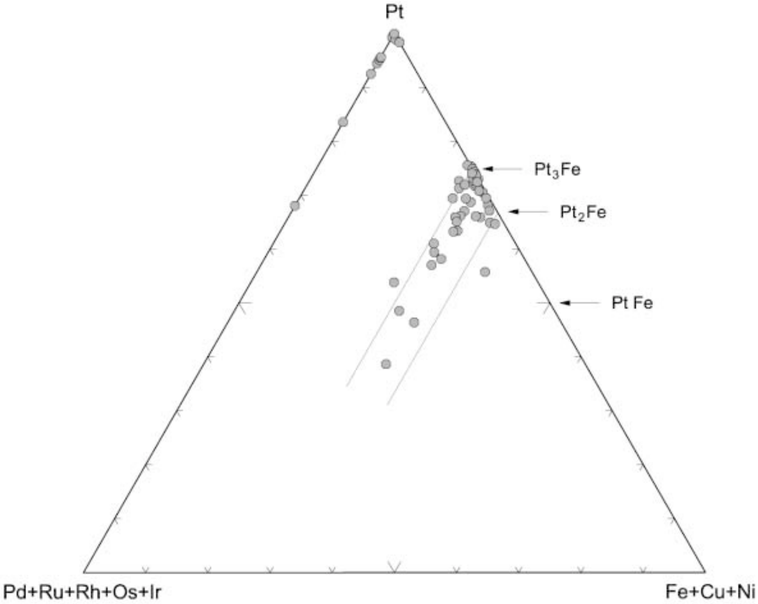

FIG. 8a. Compositions of (i) Pt, (ii) Pt–Pd alloys, (iii) Pt–Pd–Fe alloys (defined as: concentration of Pd > Ru, Rh, Os or Ir), and (iv) Pt–Fe alloys (Ru, Os or Ir < 3 at.%) projected in the triangular diagram Pt – (Pd + Ru + Rh + Os + Ir) – (Fe + Cu + Ni).

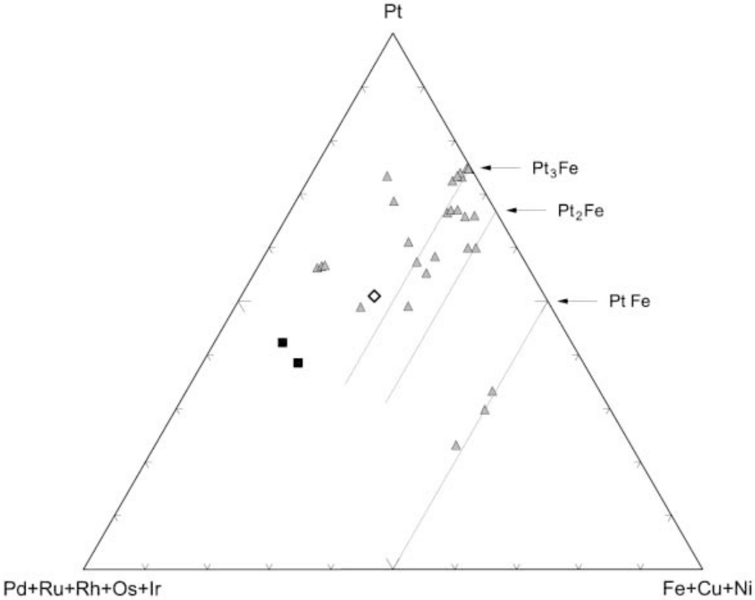

FIG. 8b. Compositions of (i) Pt–Rh–Fe alloys (concentration of Rh > Pd, Ru, Os or Ir; triangles), (ii) Pt–Ru–Fe alloys (concentration of Ru > Pd, Rh, Os or Ir; squares), and (iii) one grain with Ir > Pd, Rh, Ru or Os (diamond) projected in the triangular diagram Pt – (Pd + Ru + Rh + Os + Ir) – (Fe + Cu + Ni).

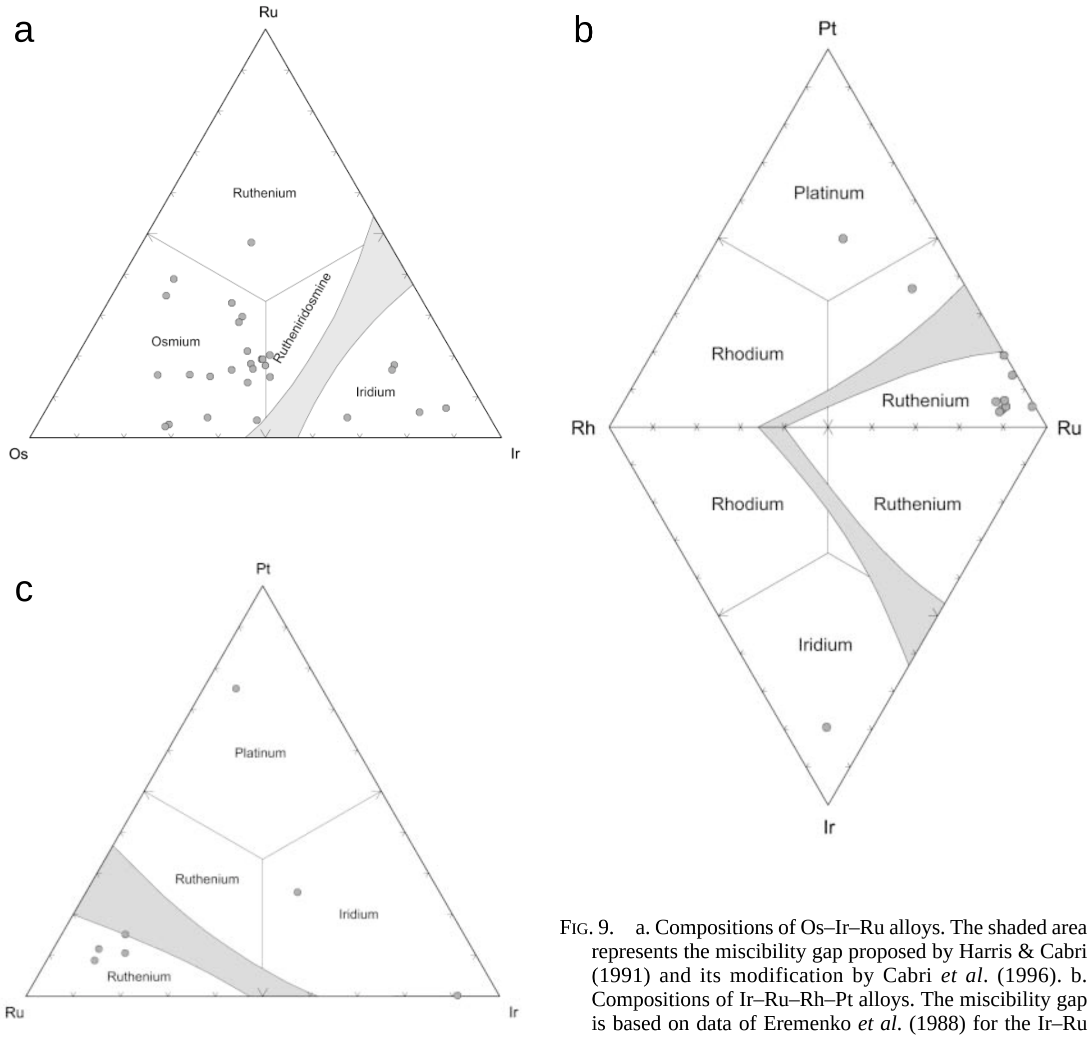

FIG. 9. a. Compositions of Os–Ir–Ru alloys. The shaded area represents the miscibility gap proposed by Harris & Cabri (1991) and its modification by Cabri *et al*. (1996). b. Compositions of Ir–Ru–Rh–Pt alloys. The miscibility gap is based on data of Eremenko *et al.* (1988) for the Ir–Ru and Pt–Ru binary alloys, and Paschoal *et al*. (1983) for the Rh–Ru binary alloys. c. Compositions of Ru–Ir–Pt alloys. The miscibility gap is based on data of Eremenko *et al.* (1988) and Cabri *et al.* (1996) for the Ru–Ir alloys, and Hutchinson (1972) for the Ru–Pt binary join.

are nearly pure ruthenium (Fig. 9b, Table 5, no. 163). The single grain in the Os–Ir–Ru diagram (Fig. 9a) has 47.8 at.% Ru, 29.1 at.% Os and 23.1 at.% Ir, as well as 4.0 wt.% Pt and traces of Rh (1.0 wt.%), Pd (0.4 wt.%), and Ni (0.15 wt.%).

The composition of iridium scatters over a wide range, with most compositions in the system Os–Ir–Ru (Fig. 9a), and single compositions in the systems Ru–Ir–Pt (Fig. 9b), Rh–Ir–Ru (Fig. 9c), Os–Ir–Pt (Table 5, no. 119), and Os–Ir–Rh (Table 5, no. 203). The grains of iridium that fall in the system Os–Ir–Ru contain between 67.1 and 84.4 at.% Ir, 8.0 and 26.3 at.% Os, and 6.5 to 20.0 wt.% Ru, up to 2.4 wt.% Pt, 0.4 wt.% Rh, and 0.7 wt.% Fe.

The two analyzed grains of rutheniridosmine have a composition similar to osmium and lie close to the boundary with osmium (Fig. 9a).

Two individual grains consist of Pt–Rh–Ru alloy with traces of Ir, Os, Fe and Cu (Table 5, no. 175), and Pt–Ru–Ir alloy with 5.0 wt.% Os, 2.5 wt.% Rh, 0.3 wt.% Pd, and 1.7 wt.% Fe (Fig. 9c).

TABLE 5. SELECTED ELECTRON-MICROPROBE DATA PERTAINING TO Os–Ir–Ru–Pt–Rh ALLOYS, SOMABULA GRAVELS, ZIMBABWE

Anal. no.	39	61	74	75	85	88	119	155	163	175	198	203
Ru wt.%	23.80	1.77	29.23	41.08	15.74	3.93	n.d.	3.48	87.14	18.19	60.56	3.66
Rh	1.91	n.d.	7.40	5.51	0.38	n.d.	n.d.	n.d.	0.68	14.24	4.47	6.04
Pd	0.26	n.d.	0.36	0.32	0.29	n.d.	n.d.	n.d.	0.29	n.d.	n.d.	n.d.
Os	57.54	69.04	10.54	22.89	11.96	8.22	36.76	26.52	n.d.	1.39	7.06	7.98
Ir	12.93	28.31	9.92	12.97	44.64	87.22	59.60	68.30	n.d.	1.98	14.42	78.02
Pt	0.84	n.d.	41.11	16.80	25.77	n.d.	2.89	n.d.	10.22	62.41	12.68	0.82
Fe	1.27	0.30	0.41	0.15	1.21	0.71	n.d.	0.32	n.d.	0.52	0.58	1.85
Cu	n.d.	n.d.	n.d.	n.d.	n.d.	n.d.	n.d.	n.d.	n.d.	0.35	n.d.	n.d.
Ni	0.18	0.21	n.d.	n.d.	0.28	0.26	n.d.	0.15	0.24	n.d.	0.15	n.d.
Total	98.73	99.63	98.97	99.72	100.27	100.34	99.25	98.77	98.57	99.08	99.92	98.37
Ru *apfu*	0.359	0.033	0.419	0.550	0.253	0.072	-	0.064	0.930	0.268	0.720	0.062
Rh	0.028	-	0.104	0.072	0.006	-	-	-	0.007	0.206	0.052	0.101
Pd	0.004	-	0.005	0.004	0.004	-	-	-	0.003	-	-	-
Os	0.461	0.674	0.080	0.163	0.102	0.081	0.373	0.259	-	0.011	0.045	0.072
Ir	0.102	0.274	0.075	0.091	0.377	0.839	0.598	0.661	-	0.015	0.090	0.701
Pt	0.007	-	0.306	0.116	0.214	-	0.029	-	0.056	0.477	0.078	0.007
Fe	0.035	0.010	0.011	0.004	0.035	0.023	-	0.011	-	0.014	0.013	0.057
Cu	-	-	-	-	-	-	-	-	-	0.008	-	-
Ni	0.005	0.008	-	-	0.008	0.008	-	0.005	0.004	-	0.001	-

n.d.: not detected, *apfu*: atoms per formula unit. Samples: 39 osmium, 61 osmium, 74 ruthenium, 75 ruthenium in the system Ru–Os–Pt, 85 iridium, 88 iridium, 119 iridium in the system Ir–Os–Pt, 155 iridium, 163 ruthenium, 175 platinum, 198 ruthenium, 203 iridium in the system Ir–Os–Rh.

Pt–Pd sulfides

PGM of the cooperite – braggite – vysotskite series are the only detrital PGE sulfides in the concentrate. There are two rounded grains, 120 and 160 μm in diameter, rich in Pd (19.2 and 31.6 wt.%), and one grain contains 0.6 wt.% Se. The corresponding formulae are $(Pt_{0.64}Pd_{0.36})_{\Sigma 1.00}(S_{0.99}Se_{0.01})_{\Sigma 1.00}$ and $(Pd_{0.54}Pt_{0.46})_{\Sigma 1.00}S_{1.00}$ (Table 5, nos. 103 and 116).

TABLE 6. SELECTED ELECTRON-MICROPROBE DATA PERTAINING TO PGE SULFIDES AND UNNNAMED PGE MINERALS, SOMABULA GRAVELS, ZIMBABWE

Anal. no.	103	116	223	224		103	116	223	224
Ru wt.%	n.d.	n.d.	2.07	n.d.	Ru	-	-	0.030	-
Rh	n.d.	n.d.	73.72	32.22	Rh	-	-	1.037	1.677
Pd	19.22	31.63	0.22	22.61	Pd	0.358	0.544	0.003	1.138
Os	n.d.	n.d.	n.d.	n.d.	Os	-	-	-	-
Ir	n.d.	n.d.	0.43	n.d.	Ir	-	-	0.003	-
Pt	62.82	48.88	2.04	5.06	Pt	0.638	0.458	0.015	0.139
Fe	n.d.	n.d.	n.d.	n.d.	Fe	-	-	-	-
Cu	n.d.	n.d.	0.21	n.d.	Cu	-	-	0.005	-
Ni	n.d.	n.d.	n.d.	n.d.	Ni	-	-	-	-
S	16.02	17.49	20.11	3.15	S	0.989	0.998	0.908	0.527
Se	0.61	n.d.	n.d.	n.d.	Se	0.015	-	-	-
Te	n.d.	n.d.	n.d.	36.16	Te	-	-	-	1.518
Total	98.06	98.00	98.80	99.20					

n.d.: not detected, *apfu*: atoms per formula unit.

Unnamed PGM

One grain of Pt–Rh–Fe alloy contains two tabular, roundish inclusions up to 20 μm long consisting of Rh (73.7 wt.%), S (20.1 wt.%), up to 2.1 wt.% Ru and 2.0 wt.% Pt (Fig. 7d). The formula $(Rh_{1.04}Ru_{0.03}Pt_{0.02})_{\Sigma 1.09}S_{0.91}$ is close to RhS (Table 6, no. 223). A PGM with a similar composition was encountered by Feather (1976) in the Witwatersrand ores, South Africa.

The same Pt–Rh–Fe alloy grain hosts a number of irregularly shaped inclusions, up to 15 μm long, rich in Rh (32.2 wt.%), Pd (22.6 wt.%), and Te (36.2 wt.%), and containing subordinate Pt (5.1 wt.%), and S (3.2 wt.%) (Table 6, no. 224). The following formula is calculated: $(Rh_{1.68}Pd_{1.14}Pt_{0.14})_{\Sigma 2.96}(Te_{1.52}S_{0.53})_{\Sigma 2.05}$ or, ideally, $(Rh,Pd)_3Te_2$. An unnamed Rh_2Te_3 was described by Hagen *et al.* (1990) in the form of drop-like inclusions in Pt–Fe alloy from placer deposits in Burma.

Os Isotope Compositions

A number of different PGM grains (Pt, Pt–Fe alloy, Pt_3Sn and Os–Ir–Ru alloy) were analyzed for their Os isotope compositions. However, only the grains of Os–Ir–Ru alloy had sufficient contents of Os to allow interpretation of the data. Os–Ir alloys are considered to be free of Re and are therefore ideal for the characterization of the Os isotope composition of their source magma (Bird *et al.* 1999).

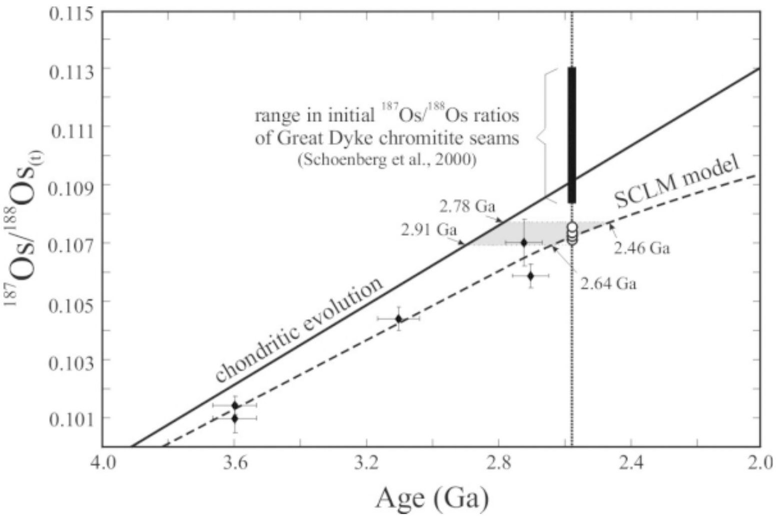

FIG. 10. Plot of initial $^{187}Os/^{188}Os$ isotope values *versus* geological age, showing the chondritic mantle evolution (bold line) and the evolution of the subcontinental lithosperic mantle (SCLM; stippled line) after Nägler *et al.* (1997). Symbols: ◆ Chromite separates from ultramafic complexes of different ages within the Zimbabwe Craton (*cf.* Nägler *et al.* 1997). ❍: Os–Ir grains from the Somabula gravels. Shaded area gives the ranges in their age following the models for the evolution of chondritic mantle and SCLM. Also shown is the range of initial $^{187}Os/^{188}Os$ values of chromite separates from various Great Dyke chromitite seams (vertical bar; Schoenberg *et al.* 1999) and the age of intrusion (dotted line = 2.58 Ga) of the Great Dyke (Mukasa *et al.* 1998, Oberthür *et al.* 2002).

TABLE 7. Os ISOTOPE COMPOSITIONS OF PGM, SOMABULA GRAVELS, ZIMBABWE

Grain	Major elements	$^{187}Os/^{188}Os$	#±
3739	Ir–Ru	0.107018	1290
3815–1	Os–Ir–Ru	0.107537	3
3815–2	Os–Ir–Ru	0.107535	3
3815–3	Os–Ir–Ru	0.107532	3
3815–4	Os–Ir–Ru	0.107540	7
	average	0.107536	7
3959–1	Os–Ir–Ru	0.107182	37
3959–2	Os–Ir–Ru	0.107230	55
3959–3	Os–Ir–Ru	0.107263	66
	average	0.107225	81
3961–1	Os–Ir–Ru	0.107074	5
3961–2	Os–Ir–Ru	0.107081	5
3961–3	Os–Ir–Ru	0.107081	11
3961–4	Os–Ir–Ru	0.107085	14
	average	0.107080	9
3978	Os–Ir–Ru	0.107118	15
3993	Os–Ir–Ru	0.120657	8

Uncertainties are given in the 95% confidence interval and refer to the last digits of the $^{187}Os/^{188}Os$ values. Uncertainties of averages are calculated as two standard deviations.

The Os–Ir–Ru alloy grains no. 3815, 3959, 3961 and 3978 form a distinct homogeneous group with respect to their $^{187}Os/^{188}Os$ values (range 0.10707–0.10754; Table 7, Fig. 10), indicative of a pristine source in the mantle. The $^{187}Os/^{188}Os$ values are significantly lower (*i.e.,* well outside the 2σ uncertainties) than the range determined for chromite separates from seams of massive chromitite in the Great Dyke (Schoenberg *et al.* 1999) (initial $^{187}Os/^{188}Os$ values between 0.1106 and 0.1126). These initial Os compositions are just slightly above the value of the contemporaneous chondritic mantle, 0.1094 (Shirey & Walker 1998). In addition, an Os isotope analysis of one detrital Os–Ir–Ru alloy grain from a river draining the Great Dyke gave an $^{187}Os/^{188}Os$ value of 0.110275 (J.D. Kramers, written commun., 2001), well in the range of initial $^{187}Os/^{188}Os$ values (average 0.1112) of the chromitites of the Great Dyke.

The maximum values for the initial $^{187}Os/^{188}Os$ signature of the Somabula PGM grains are significantly lower (*i.e.,* well outside the 2σ uncertainty limits) than the initial Os-isotope composition of the Great Dyke magma. Therefore, a derivation of the Os–Ir–Ru grains from the Great Dyke is precluded (Fig. 10). Depending on the model used, the grains either originate from a mafic–ultramafic complex 2.91 to 2.78 Ga old derived from a chondritic mantle, or from a mafic–ultramafic intrusion 2.64 to 2.46 Ga old with Os characteristics of the subcontinental lithospheric mantle (SCLM). Notably, all greenstone belts of the Zimbabwe craton investigated by Nägler *et al*. (1997) clearly reflect Os signatures from the SCLM.

Grain 3993 displays a somewhat higher $^{187}Os/^{188}Os$ value, 0.12067. It is not clear whether the evolved Os-isotope composition of grain 3993, compared to that of the other Os–Ir–Ru grains, is due to *in situ* growth of Re, reveals another magmatic source, or is a combination of both.

In conclusion, the Os isotope compositions of detrital Os–Ir–Ru grains are useful tracers of their origin. The Os isotope compositions of the Os–Ir–Ru grains from Somabula point to a source of the Os in the pristine mantle. Furthermore, derivation of these grains from the Great Dyke appears improbable; rather, they originate from ultramafic–mafic rocks in late Archean greenstone belts of the Zimbabwe craton.

DISCUSSION AND CONCLUSIONS

Source-area aspects

The polymict spectrum of heavy minerals in the Somabula paleoplacers indicates lithologically complex source-areas. Unfortunately, there are no direct clues to the hinterland exposed in Karoo times, some 200 Ma ago, and probably eroded now. It is beyond the scope of this paper to relate all heavy minerals to specific sources. However, some evidence gained during the study will be discussed in order to show the complexity of this paleoplacer.

The ubiquitous staurolite suggests an amphibolite-facies metamorphic source-terrane. The mineral is widespread in northern Zimbabwe only, in the Miami mica fields (Fig. 11), in the Urungwe, Mount Darwin and Mtoko areas (Warner 1972).

The age range of most zircon, monazite and columbite–tantalite grains matches that of Pan-African rocks. Since almost all of the zircon and monazite is similar in appearance, these ages may be typical of the whole population. The calculated Th/U values are indicative of a probable magmatic, rather than metamorphic, origin for both zircon and monazite. The high abundance of monazite suggests that the source rocks were formed from crustal melts, such as S-type granitic rocks. The presence of abundant detrital monazite, which is a relatively soft, easily abraded mineral, suggests that the Pan-African source was not very distant. The Pan-African Mozambique and Zambezi belts to the east and north (Fig. 11) are potential sources. These results suggest that part of the Pan-African belts near Zimbabwe formed a high-standing terrain during the Triassic when the sediment was eroded and transported.

Cassiterite and uraninite probably originate from granitic rocks and associated pegmatites of unknown age. Magnetite and hematite have many possible origins, and may have been derived from banded iron-formations, prominent in the Archean greenstone belts of the Zimbabwe craton. The most probable source of native gold has to be sought in areas of hydrothermal mineralization, abundant in the Archean greenstone belts exposed in proximity of Somabula (Figs. 1, 11). The diamond crystals probably have their origin in kimberlites. Notably, kimberlite pipes occur some 50–100 km to the southwest of Somabula, and also in the Limpopo belt (Fig. 11).

In conclusion, the wide spectrum of heavy minerals in the Somabula placers and the specific data collected in this study indicate a diversity of source lithologies. Repeated stages of reworking have to be envisaged, and the various components from specific sources may have been added to the heavy-mineral spectrum at any time during the prolonged history of the sediment. Furthermore, the Pan-African ages of some minerals suggest that part of the Pan-African belts to the north and east of the Zimbabwe craton formed a high-standing terrain during the Triassic when the sediment was eroded and transported.

Platinum-group minerals

The PGM assemblage found in the Somabula placers is distinctly different from the PGM of the Main Sulfide Zone of the Great Dyke (dominantely Pt,Pd bismuthotellurides, sperrylite and cooperite–braggite; Farahmand 1974, Johan *et al.* 1989, Coghill & Wilson 1993, Oberthür *et al.* 1998, Weiser *et al.* 1998), and the detrital PGM originating from the Great Dyke (mainly sperrylite, Pt and Pt–Fe alloys; Oberthür *et al.* 1998, 1999). Futhermore, the Os isotope compositions of the Os-rich grains from Somabula suggest that their source rocks such as ultramafic–mafic rock successions or intrusions of late Archean age of the Zimbabwe craton were derived from the mantle, without crustal contamination. The Os isotope ratios rule out the possibility that the Somabula PGM were derived from the Great Dyke.

However, the combination of unknown sources, unknown events of weathering and sedimentary transport, and unknown post-depositional history of the placers, pose severe problems in pointing to specific sources of the PGM. Mertie (1969) reported that platinum alloys rarely migrate far downstream from their bedrock sources, unless they are so fine-grained as to be moved by swift water or floated by surface tension. Thus, except for unusual situations (*e.g.*, glaciation), placers of the precious metals may be assumed to lie within a few km of their bedrock sources (Mertie 1969). Most of the PGM at Somabula appear to be original grains that have experienced only subordinate chemical and physical alteration during transport and following deposition. Therefore, the sizes of the PGM grains (between 100 and 850 μm) favor transport as bedload, not in suspension, and according to Mertie (1969) would point to source rocks relatively close to Somabula (up to some tens of km).

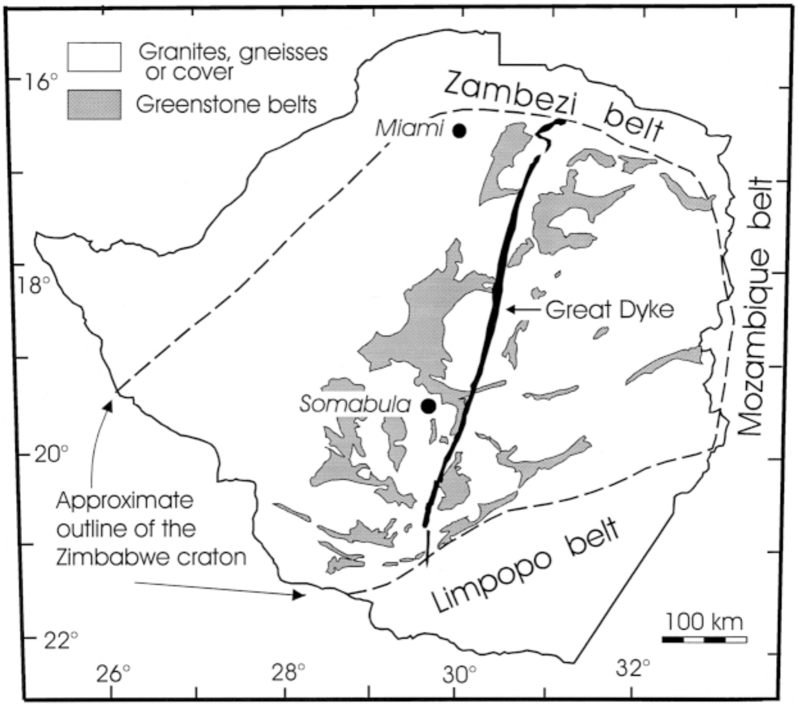

FIG. 11. Simplified geological map of Zimbabwe showing an outline of the Zimbabwe craton, Archean greenstone belts, the Great Dyke, and adjacent mobile belts. Locations of Somabula and Miami are shown by dots (•).

The overall PGM assemblage, *ca.* 90% Pt-rich minerals and 10% Os–Ir–Ru–Rh–Pt alloys, is grossly comparable to that of many modern placers that have primary sources in Alaskan or Alpine-type mafic–ultramafic complexes (*e.g.,* Cabri *et al.* 1996). Notable at Somabula are (i) the near-absence of platinum-group element (PGE) sulfides, (ii) the exceptional compositions of Pt and Pt alloy grains with Pd, Rh or Ru, (iii) the wide range of compositions of the Os–Ir–Ru–Rh–Pt alloy grains, (iv) the presence of Pt–Pd–Au alloys, and (iv) the presence of rustenburgite, not yet reported to be so prevalent from placers.

Textures of PGM at Somabula, their intergrowths and inclusions, the specific compositions of minerals of multicomponent Pt and Os–Ir–Ru–Rh–Pt alloys, and the Os isotope compositions, provide evidence of a high-temperature, magmatic origin of most of the PGM grains. Only the grains of pure Pt, and the rhythmically zoned, porous Pt–Pd alloys, may have formed by the dissolution of less stable PGE-bearing phases or PGM and subsequent reprecipitation of Pt or Pd at ambient temperatures, in the weathering environment. Also, changes during weathering, fluvial transport or by groundwaters after deposition may have to be taken into account, and both leaching and accretion may have taken place (Cousins & Kinloch 1976, Bowles 1986, 1995, Augé *et al.* 1995, Cabri *et al.* 1996).

The near-absence of PGE sulfides as detrital grains and as inclusions in other PGM may point to a primary ore-forming environment of low sulfur fugacity. Alternatively, PGE sulfides may have been destroyed during weathering and fluvial transport. However, the absence of inclusions of PGE sulfides, the presence of Ru-rich alloy, and at the same time the absence of laurite, contradict the hypothesis that PGE sulfides were originally more common in the source rocks. Therefore, the PGM assemblage most probably represents PGM grains that formed at magmatic conditions in low-sulfur mafic–ultramafic rocks or chromitites, whereas a derivation from magmatic Ni-sulfide deposits may be ruled out.

The multicomponent alloys of Pt with Pd, Rh and Ru probably formed from complex PGE-dominant solid solutions at low sulfur fugacities and at magmatic temperatures. In case of elevated sulfur fugacities, one would expect that the large proportions of Rh, Ru and Ir found in many of the alloys would form sulfides, but these are missing at Somabula. Similarly, the Os–Ir–Ru–Rh–Pt alloys, which display a wide scatter of compositions, indicate that they formed from complex PGE-dominant solid solutions. The Os isotope compositions of Os-rich grains point to a pristine mantle source. We therefore suggest that basic–ultrabasic rocks, possibly komatiites, represent the likely magmatic environments in which these PGM formed.

Pt–Pd–Au solid solutions are only stable above 1050°C (Hansen & Anderko 1958). Therefore, the presence of such alloys at Somabula indicates that they formed in a magmatic environment. Rustenburgite is a rare primary PGM, *e.g.*, in the magmatic ores of the Bushveld Complex in South Africa (Mihálik *et al.* 1975) and the Norilsk deposit in Russia (Distler *et al.* 1993), but had until now been unknown as a ubiquitous detrital constituent of placer deposits. Our limited knowledge on the mode of formation and stability of rustenburgite only allows us to loosely link this mineral to primary magmatic ore-forming environments. However, the occasional intergrowths of rustenburgite and Pt alloys indicates a common genesis and high-temperature formation of these PGM.

In conclusion, except perhaps for the Pt and Pt–Pd alloy grains, most of the PGM grains at Somabula have experienced only subordinate chemical and physical alteration prior to and following their deposition. Os isotope compositions of Os–Ir–Ru alloys indicate pristine mantle sources and no crustal contamination. Textures of PGM at Somabula, their intergrowths and inclusions, the specific mineral chemistry and the compositions of the multicomponent Pt and Os–Ir–Ru–Rh–Pt alloys are interpreted to point to the formation of most of the PGM grains at magmatic temperatures. The assemblage of detrital PGM found at Somabula most probably originates from low-sulfur mafic–ultramafic rocks, possibly of komatiite affinity, which are widespread lithologies in the Archean greenstone belts of Zimbabwe.

Acknowledgements

Sincere thanks go to the former mine manager, Stephen Annandale, for allowing us to sample the last existing mineral concentrate of the Somabula mining operations. J.H.G. Laflamme of CANMET mounted the individual PGM grains and prepared excellent polished sections. We also thank J. Lodziak (BGR) for carrying out the electron-microprobe analyses, and Figure 1 was ably drafted by Ms. Souto (BGR). L.J. Cabri (Ottawa), T. Blenkinsop (Harare), and F. Melcher (BGR) provided constructive comments on an earlier version of this paper. Further suggestions by H.-G. Bachmann, K.-P. Burgath (BGR) and T.L. Evstigneeva (IGEM, Moscow) are gratefully acknowledged. Valuable comments of referees K. Hattori (Ottawa), A.Y. Barkov (Montreal), an anonymous referee and the editor, R.F. Martin, considerably improved the final version of the paper.

We are happy to contribute to this volume dedicated to Louis J. Cabri. Over many years, it was for us a great pleasure to cooperate with him in the field of noble metals, especially the PGE. We learned a great deal from him; our collaboration led to a considerable joint output.

References

Augé, T., Maurizot, P., Breton, J., Eberlé, J.M., Gilles, C., Jézéquel, P., Mézière, J. & Robert, M. (1995): Magmatic and supergene platinum-group minerals in the New Caledonia ophiolite. *In* Platinum Group Elements in Supergene Processes (T. Augé & E. Stumpfl, eds.). *Chron. Rech. Minières* **63**(520), 3-26.

Bird, J.M., Meibom, A., Frei, R. & Nägler, T.F. (1999): Osmium and lead isotopes of rare OsIrRu minerals: derivation from the core–mantle boundary region? *Earth Planet. Sci. Lett.* **170**, 83-92.

Bowles, J.F.W. (1986): The development of platinum-group minerals in laterites. *Econ. Geol.* **81**, 1278-1285.

________ (1995): The development of platinum-group minerals (PGM) in laterites: mineral morphology. *Chron. Rech. Minières* **520**, 55-63.

Bucher, K. & Frey M. (1994): *Petrogenesis of Metamorphic Rocks.* Springer-Verlag, Berlin, Germany.

Bührmann, H.T. (1997): Somabula Diamond Project – Zimbabwe. Final report on exploration programme of Trans Hex Group Limited, EPO 771 & 808. *Arch. Geol. Surv. Zimbabwe, Harare, Zimbabwe.*

Cabri, L.J., Harris, D.C. & Weiser, T.W. (1996): The mineralogy and distribution of platinum group mineral (PGM) placer deposits of the world. *Explor. Mining Geol.* **5**, 73-167.

Coghill, B.M. & Wilson, A.H. (1993): Platinum-group minerals in the Selukwe subchamber, Great Dyke, Zimbabwe: implications for PGE collection mechanisms and post-formational redistribution. *Mineral. Mag.* **57**, 613-633.

Cousins, C.A. & Kinloch, E.D. (1976): Some observations on textures and inclusions in alluvial platinoids. *Econ. Geol.* **71**, 1377-1398.

Distler, V.V., Dyuzhikov, O.A. & Genkin, A.D. (1993): The Talnakh ore field: a copper – nickel – platinum giant. *Geology of Ore Deposits* **35**, 1-13.

Eremenko, V.N., Khoruzhaya, V.G. & Shtepa, T.D. (1988): Temperature of nonvariant equilibria in the systems Zr–Ru and Ru–Ir. *Russian Metall. (Metally)* **1988**(1), 194-198.

Farahmand, A. (1974): *Sulfiderze des Great Dyke (Rhodesien) und die hydrometallurgische Gewinnbarkeit ihrer Wertmetalle.* Dissertation (Dr.-Ing.), Technical University Berlin, Berlin, Germany.

Feather, C.E. (1976): Mineralogy of platinum-group minerals in the Witwatersrand, South Africa. *Econ. Geol.* **71**, 1399-1428.

GIBSON, C.A. (1967): Final report of Somabula diamond field. Rio Tinto, EPO 182. *Arch. Geol. Surv. Zimbabwe, Harare, Zimbabwe*.

HAGEN, D., WEISER, T. & THAN HTAY (1990): Platinum-group minerals in Quaternary gold placers in the upper Chindwin area of northern Burma. *Mineral. Petrol.* **42**, 265-286.

HANSEN, M. & ANDERKO, K. (1958): *Constitution of Binary Alloys*. McGraw-Hill, New York, N.Y.

HARRIS, D.C. & CABRI, L.J. (1991): Nomenclature of platinum-group element alloys: review and revision. *Can. Mineral*. **29**, 231-237.

HARRISON, N.M. (1980): The Somabula diamond fields. *Rhod. Geol. Surv., Tech. Files*, 1-3.

HUTCHINSON, J.M. (1972): Solubility relationships in the ruthenium–platinum system. *Plat. Metals Rev*. **16**, 88-90.

JAFFEY, A.H., FLYNN, K.F., GLENDENNIN, L.E., BENTLEY, W.C. & ESSLING, A.M. (1971): Precision measurement of half-lives and specific activities of ^{235}U and ^{238}U. *Phys. Rev*. **4**, 1889-1906.

JOHAN, Z., OHNENSTETTER, D. & NALDRETT, A.J. (1989): Platinum-group minerals and associated oxides and base metal sulphides of the Main Sulphide Zone, Great Dyke, Zimbabwe. *In* Fifth Int. Platinum Symp. (H. Papunen, ed.). *Bull. Geol. Soc. Finland* **61**(1), 53-54.

KROGH, T.E. (1973): A low contamination method for the hydrothermal decomposition of zircon and extraction of U and Pb for isotopic age determinations. *Geochim. Cosmochim. Acta* **37**, 485-494.

MACGREGOR, A.M. (1941): Gorceixite in Southern Rhodesia. *Bulletin of the Imperial Institute* **39**(4), 399-401.

________ & ZEALLEY, A.E.V. (1921): The geology of the diamond-bearing gravels of the Somabula Forest. *S. Rhodesia Geol. Surv., Bull.* **8**, 1-38.

MASTER, S. (1995): A review and re-appraisal of ideas concerning the source of diamonds in the Triassic Somabhula gravels, Zimbabwe. *In* Sub-Saharan Economic Geology (T.G. Blenkinsop & P.L. Tromp, eds.). A.A. Balkema, Rotterdam, The Netherlands (161-176).

MATTHEWS, W. & DAVIS, W.J. (1999): A practical image analysis technique for estimating the weight of abraded mineral fractions used in U–Pb dating. *In* Radiogenic Age and Isotopic Studies: Report 12. *Geol. Surv. Can., Current Research* **1999-F**, 1-7.

MERTIE, J.B. (1969): Economic geology of the platinum metals. *U. S. Geol. Surv., Prof. Pap.* **630**, 1-120.

MIHÁLIK, P., HIEMSTRA, S.A. & DE VILLIERS, J.P.R. (1975): Rustenburgite and atokite, two new platinum-group minerals from the Merensky Reef, Bushveld Igneous Complex. *Can. Mineral.* **13**, 146-150.

MUKASA, S.B., WILSON, A.H. & CARLSON, R.W. (1998): A multielement geochronologic study of the Great Dyke, Zimbabwe: significance of the robust and reset ages. *Earth Planet. Sci. Lett.* **164**, 353-369.

NÄGLER, T.F. & FREI, R. (1997): ”Plug in” Os distillation. *Schweiz. Mineral. Petrogr. Mitt.* **77**, 123-127.

________, KRAMERS, J.D., KAMBER, B.S., FREI, R. & PRENDERGAST, M.D.A. (1997): Growth of subcontinental lithospheric mantle beneath Zimbabwe started at or before 3.8 Ga: Re–Os study on chromites. *Geology* **25**, 983-986.

NIER, A.O. (1937): The isotopic constitution of osmium. *Phys. Rev.* **52**, 885.

OBERTHÜR, T., DAVIS, D.W., BLENKINSOP, T.G. & HÖHNDORF, A. (2002): Precise U–Pb mineral ages, Rb–Sr and Sm–Nd systematics for the Great Dyke, Zimbabwe – constraints on late Archean events in the Zimbabwe Craton and Limpopo Belt. *Precamb. Res.* **113**, 293-305.

________, WEISER, T. & GAST, L. (1999): Mobility of PGE and PGM in the supergene environment at Hartley mine, Great Dyke, Zimbabwe – a case study. *In* Mineral Deposits: Processes to Processing (C.J. Stanley *et al*., eds.). A.A. Balkema, Rotterdam, The Netherlands (763-766).

________, ________, ________, LODZIAK, J., KLOSA, D. & WITTICH, C. (1998): Detrital platinum group minerals in rivers along the Great Dyke, and in the Somabula gravels, Zimbabwe. *In* Eighth Int. Platinum Symp. *S. Afr. Inst. Mining Metall., Symp. Ser.* **S 18**, 289-292.

PASCHOAL, J.O.A., KLEYKAMP, H. & THÜMMLER, F. (1983): Phase equilibria in the quaternary molybdenum – ruthenium – rhodium – palladium system. *Z. Metallkunde* **74**, 652-353.

PHAUP, A.E. (1958): History of the Somabula diamond field, Willoughbys Siding. *Rhod. Geol. Surv., Tech. Files.*

POUCHOU, J.-L. & PICHOIR, F. (1991): Quantitative analysis of homogeneous or stratified microvolumes applying the model “PAP“ in microprobe analysis. *In* Electron Probe Quantitation (K.F.J. Heinrich & D.E Newbury, eds.). Plenum Press, New York, N.Y. (31-75).

ROMER, R.L. & SMEDS, S.-A. (1996): U–Pb columbite ages of pegmatites from Sveconorwegian terranes in southwestern Sweden. *Precamb. Res.* **76**, 15-30.

SCHOENBERG, R., NÄGLER, T.F. & KRAMERS, J.D. (1999): On the source of the Great Dyke layered ultramafic to mafic intrusion, Zimbabwe: a Re–Os study on chromites. *EUG J. Conf. Abstr.* **4**, 804.

________, ________ & ________ (2000): Precise Os isotope and Re–Os isotope dilution measurements down to the picogram level using multicollector inductively coupled plasma mass spectrometry. *Int. J. Mass Spectr.* **197**, 85-94.

SEWARD, A.C. & HOLTTUM, B.A. (1921): On a collection of fossil plants from Southern Rhodesia. *S. Rhodesia Geol. Surv., Bull.* **8**, 39-45.

SHIREY, S.B. & WALKER, R.J. (1998): ^{187}Re/^{187}Os isotopes in cosmochemistry and high-temperature geochemistry. *Annu. Rev. Earth Planet. Sci.* **26**, 423-500.

STACEY, J.S. & KRAMERS, J.D. (1975): Approximation of terrestrial lead isotope evolution by a two-stage model. *Earth Planet. Sci. Lett.* **26**, 207-221.

TOLSTYKH, N.D., LAPUKHOV, A.S., KRIVENKO, A.P. & LAZAREVA, E.V. (1999): Platinum-group minerals in gold placers in northwestern Salair. *Russ. Geol. Geophys.* **40**, 916-925.

TÖRNROOS, R., JOHANSON, B. & KOJONEN, K. (1998): Alluvial nuggets of platinum-group minerals and alloys from Finnish Lapland. *Geol. Surv. Finland, Spec. Pap*. **26**, 63-64.

TYNDALE-BISCOE, R. (1949): The geology of the country around Gwelo. *S. Rhod. Geol. Surv., Bull.* **39**.

WARNER, S.M. (1972): Check list of the minerals of Rhodesia. *Rhodesia Geol. Surv. Bull.* **69**, 72.

WEISER, T., OBERTHÜR, T., KOJONEN, K. & JOHANSON, B. (1998): Distribution of trace PGE in pentlandite and of PGM in the Main Sulfide Zone (MSZ) at Mimosa mine, Great Dyke, Zimbabwe. *In* Eighth Int. Platinum Symp. *S. Afr. Inst. Mining Metall., Symp. Ser.* **S 18**, 443-445.

WILSON, J.F., NESBITT, R.W. & FANNING, C.M. (1995): Zircon geochronology of Archaean felsic sequences in the Zimbabwe Craton: a revision of greenstone stratigraphy and a model for crustal growth. *In* Early Precambrian Processes (M.P. Coward & A.C. Ries, eds.). *Geol. Soc., Spec. Publ*. **95**, 109-126.

Received September 8, 2000, revised manuscript accepted March 15, 2002.